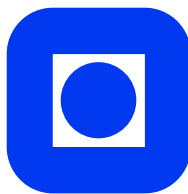


Criticality and novel quantum liquid phases in Ginzburg–Landau theories with compact and non-compact gauge fields

by
Jo Smiseth

Thesis submitted in partial fulfillment of the requirements for the Norwegian academic degree of Doktor Ingeniør



Department of Physics
Norwegian University of Science and Technology
Trondheim, Norway

August, 2005

Abstract

We have studied the critical properties of three-dimensional U(1)-symmetric lattice gauge theories. The models apply to various physical systems such as insulating phases of strongly correlated electron systems as well as superconducting and superfluid states of liquid metallic hydrogen under extreme pressures. This thesis contains an introductory part and a collection of research papers of which seven are published works and one is submitted for publication.

Paper I: Critical properties of the 2+1-dimensional compact abelian Higgs model with gauge charge $q = 2$ are studied. We introduce a novel method of computing the third moment M_3 of the action which allows us to extract correlation length and specific heat critical exponents ν and α without invoking hyperscaling. Finite-size scaling analysis of M_3 yields the ratio $(1 + \alpha)/\nu$ and $1/\nu$ separately. We find that α and ν vary along the critical line of the theory, which however exhibits a remarkable resilience of Z_2 criticality. We conclude that the model is a fixed-line theory, which we propose to characterize the zero temperature quantum phase transition from a Mott-Hubbard insulator to a charge-fractionalized insulator in two spatial dimensions.

Paper II: Large scale Monte Carlo simulations are employed to study phase transitions in the three-dimensional compact abelian Higgs model in adjoint representations of the matter field, labeled by an integer q , for $q = 2, 3, 4, 5$. We also study various limiting cases of the model, such as the Z_q lattice gauge theory, dual to the 3D Z_q spin model, and the 3D xy spin model which is dual to the Z_q lattice gauge theory in the limit $q \rightarrow \infty$. In addition, for benchmark purposes, we study the 2D square lattice 8-vertex model, which is exactly solvable and features non-universal critical exponents. The critical exponents α and ν are calculated from finite size scaling of the third moment of the action, and the method is tested thoroughly on models with known values for these exponents. We have found that for $q = 3$, the three-dimensional compact abelian Higgs model exhibits a second order phase transition line which joins a first order phase transition line at a tricritical point. The results for $q = 2$ in Paper I are reported with a higher lever of detail.

Paper III: This paper is based on a talk by F. S. Nogueira in the Aachen HEP 2003 conference where a review of the results for the compact abelian Higgs model from Paper I and Paper II was presented, as well as the results for the $q = 1$ case studied by F. S. Nogueira, H. Kleinert and A. Sudbø.

Paper IV: We study the effects of a Chern-Simons (CS) term in the phase structure of two different abelian gauge theories in three dimensions. By duality transformations we show how the compact U(1) gauge theory with a CS term for certain values of the CS coupling can be written as a gas of vortex loops interacting through steric repulsion.

This theory is known to exhibit a phase transition governed by proliferation of vortex loops. We also employ Monte Carlo simulations to study the non-compact $U(1)$ abelian Higgs model with a CS term. Finite size scaling of the third moment of the action yields critical exponents α and ν that vary continuously with the strength of the CS term, and a comparison with available analytical results is made.

Paper V: The critical properties of N -component Ginzburg-Landau theory are studied in $d = 2 + 1$ dimensions. The model is dualized to a theory of N vortex fields interacting through a Coulomb and a screened potential. The model with $N = 2$ shows two anomalies in the specific heat. From Monte Carlo simulations we calculate the critical exponents α and ν and the mass of the gauge field. We conclude that one anomaly corresponds to an *inverted* 3D xy fixed point, while the other corresponds to a 3D xy fixed point. There are N fixed points, namely one corresponding to an inverted 3D xy fixed point, and $N - 1$ corresponding to neutral 3D xy fixed points. Applications are briefly discussed.

Paper VI: The phase diagram and critical properties of the N -component London superconductor are studied both analytically and through large-scale Monte-Carlo simulations in $d = 2 + 1$ dimensions. The model with different bare phase stiffnesses for each flavor is a model of superconductivity which should arise out of metallic phases of light atoms under extreme pressure. A projected mixture of electronic and protonic condensates in liquid metallic hydrogen under extreme pressure is the simplest example, corresponding to $N = 2$ with individually conserved matter fields. We compute critical exponents α and ν for $N = 2$ and $N = 3$. The results from Paper V are presented at a higher level of detail. For the arbitrary N case, there are N fixed points, namely one charged inverted 3D xy fixed point, and $N - 1$ neutral 3D xy fixed points. We explicitly identify one charged vortex mode and $N - 1$ neutral vortex modes. The model for $N = 2$ and equal bare phase stiffnesses corresponds to a field theoretical description of an easy-plane quantum antiferromagnet. In this case, the critical exponents are computed and found to be non 3D xy values. Furthermore, we study the model in an external magnetic field, and find a novel feature, namely $N - 1$ superfluid phases arising out of N charged condensates. In particular, for $N = 2$ we point out the possibility of two novel types of field-induced phase transitions in ordered quantum fluids: *i)* A phase transition from a superconductor to a superfluid or vice versa, driven by tuning an external magnetic field. *This identifies the superconducting phase of liquid metallic hydrogen as a novel quantum fluid.* *ii)* A phase transition corresponding to a quantum fluid analogue of sublattice melting, where a composite field-induced Abrikosov vortex lattice is decomposed and disorders the phases of the constituent condensate with lowest bare phase stiffness. Both transitions belong to the 3D xy universality class.

Paper VII: We consider the vortex superconductor with two individually conserved condensates in a finite magnetic field. The ground state is a lattice of cocentered vortices in both order parameters. We find two novel phase transitions when temperature is

increased at fixed magnetic field. *i)* A “vortex sublattice melting” transition where vortices in the field with lowest phase stiffness (“light vortices”) lose cocentricity with the vortices with large phase stiffness (“heavy vortices”), entering a liquid state (the structure factor of the light vortex sublattice vanishes *continuously*.) This transition is in the 3D xy universality class. *ii)* A first order melting transition of the lattice of heavy vortices in a liquid of light vortices.

Paper VIII: We report on large-scale Monte Carlo simulations of a novel type of a vortex matter phase transition which should take place in a three dimensional two-component superconductor. We identify the regime where first, at a certain temperature a field-induced lattice of co-centered vortices of both order parameters melts, causing the system to lose superconductivity. In this state the two-gap system retains a broken composite symmetry and we observe that at a higher temperature it undergoes an extra phase transition where the disordered composite one-flux-quantum vortex lines are “ionized” into a “plasma” of constituent fractional flux vortex lines in individual order parameters. This is the hallmark of the superconductor-to-superfluid-to-normal fluid phase transitions projected to occur in e.g. liquid metallic hydrogen.

Acknowledgments

First of all I want to express my deepest gratitude to Professor Asle Sudbø who has been my supervisor throughout this work. His genuine interest in physics as well as his enthusiastic supervision during the entire period has been very stimulating. With great physical insight and intuition he has given me very interesting problems to work on. Whenever I have presented questions or topics to discuss he has always generously spent time resolving the issues. Moreover, I am very thankful for the many fruitful and inspiring summer schools and meetings abroad which he has encouraged me to attend. Working under his supervision has been highly rewarding.

Warm thanks go to Eivind Smørgrav with whom I have cooperated closely during this work. I have enjoyed all the physics discussions, the Monte Carlo simulations and programming, writing articles together, as well as the marvelous dinners with Hege, Hanne, and Vetle. It has been a true pleasure to work with him.

I want to thank Egor Babaev for many good physics discussions and for generously telling me about vortex physics, liquid metallic hydrogen and techniques used for measurements at extreme pressures. I also want to thank Professor N. W. Ashcroft for stimulating discussions on the topic of liquid metallic hydrogen.

Furthermore, I want to express thanks to Joakim Hove who helped me with all kinds of problems in the beginning of this work, ranging from parallel computer programming to physics. Moreover, I thank Flavio Nogueira and Sjur Mo for physics discussions. I want to express thanks to Kari Rummukainen who provided the invaluable Ferrenberg-Swendsen reweighting program which was applied in this work.

I would like to thank Martin Grønsløth, Stein Olav Skrøvseth, Jan Petter Morten, Daniel Huertas-Hernando, Steinar Kragset, Kjetil Børkje, Eskil Kulseth Dahl, Jan Øystein Haavig Bakke, Per Kristian Hove, Terje Røsten, and Anh Kiet Nguyen for great discussions about physics, programming, and life, and for providing a great atmosphere at the fantastic coffee meetings. I also want to thank Terje Røsten for constant computer support and for valuable help with The Visualization Toolkit which enabled 3D vortex visualization. Moreover, I thank Steinar Kragset for proofreading this document. Many thanks also go to Martin Grønsløth, Edrun Andrea Schnell, and many of the above for invaluable help with the complete makeover of my kitchen and living room with scale invariant half millimeter precision.

The Norwegian University of Science and Technology (NTNU) is gratefully acknowledged for providing the financial support for this work through a university fellowship. Moreover, I thank NTNU and The Research Council of Norway for providing the vast amounts of computation time on the SGI Origin 3800 parallel computers which were used in this work. I also want to thank Nordita for support for several summer schools and meetings.

Finally, I would like to thank my family for all their support.

List of papers

- Paper I, Reference [1]:** A. Sudbø, E. Smørgrav, J. Smiseth, F. S. Nogueira, and J. Hove,
Criticality in the (2+1)-Dimensional Compact Higgs Model and Fractionalized Insulators,
Physical Review Letters **89**, 226403 (2002)
- Paper II, Reference [2]:** J. Smiseth, E. Smørgrav, F. S. Nogueira, J. Hove, and A. Sudbø,
Phase structure of (2+1)-dimensional compact lattice gauge theories and the transition from Mott insulator to fractionalized insulator,
Physical Review B **67**, 205104 (2003)
- Paper III, Reference [3]:** F. S. Nogueira, J. Smiseth, E. Smørgrav, and A. Sudbø,
Compact $U(1)$ gauge theories in 2+1 dimensions and the physics of low dimensional insulating materials,
European Physical Journal C **33**, 885-889 (2004)
- Paper IV, Reference [4]:** E. Smørgrav, J. Smiseth, A. Sudbø, and F. S. Nogueira,
Phase structure of Abelian Chern-Simons gauge theories,
Europhysics Letters **68**, 198-204 (2004)
- Paper V, Reference [5]:** J. Smiseth, E. Smørgrav, and A. Sudbø,
Critical Properties of the N -Color London Model,
Physical Review Letters **93**, 077002 (2004)
- Paper VI, Reference [6]:** J. Smiseth, E. Smørgrav, E. Babaev and A. Sudbø,
Field- and temperature induced topological phase transitions in the three-dimensional N -component London superconductor,
Physical Review B **71**, 214509 (2005)
- Paper VII, Reference [7]:** E. Smørgrav, J. Smiseth, E. Babaev, and A. Sudbø,
Vortex Sublattice Melting in a Two-Component Superconductor,
Physical Review Letters **94**, 096401 (2005)
- Paper VIII, Reference [8]:** E. Smørgrav, E. Babaev, J. Smiseth, and A. Sudbø,
Observation of a metallic superfluid in a numerical experiment,
submitted to Physical Review Letters (2005)

My contributions to the papers

- Paper I:** *Criticality in the (2+1)-Dimensional Compact Higgs Model and Fractionalized Insulators.* I wrote the code, performed the Monte Carlo simulations, did the data analysis, and developed the third moment of the action method in close collaboration with Eivind Smørgrav. Moreover, I was involved in writing the paper, especially in reporting results.
- Paper II:** *Phase structure of (2+1)-dimensional compact lattice gauge theories and the transition from Mott insulator to fractionalized insulator.* I wrote the code, performed the Monte Carlo simulations, did the data analysis, and developed and benchmarked the third moment of the action method in close collaboration with Eivind Smørgrav. Moreover, I wrote parts of the paper, I was especially involved in Sections III and IV.
- Paper III:** *Compact $U(1)$ gauge theories in 2+1 dimensions and the physics of low dimensional insulating materials.* I wrote the code, performed the Monte Carlo simulations and did the data analysis in close collaboration with Eivind Smørgrav.
- Paper IV:** *Phase structure of Abelian Chern-Simons gauge theories.* I wrote the code, performed the Monte Carlo simulations and did the data analysis in close collaboration with Eivind Smørgrav. I wrote the paper in close collaboration with Eivind Smørgrav.
- Paper V:** *Critical Properties of the N -Color London Model.* I wrote the code, performed the Monte Carlo simulations and did the data analysis in close collaboration with Eivind Smørgrav. My contribution also involved the exact analytical dualization of the multi-component vortex-vortex interaction. I was highly involved in writing all parts of the paper.
- Paper VI:** *Field- and temperature induced topological phase transitions in the three-dimensional N -component London superconductor.* I wrote the code, performed the Monte Carlo simulations and did the data analysis in close collaboration with Eivind Smørgrav. My contribution also involved the exact analytical dualization of the multi-component vortex-vortex interaction which is reported in detail in Appendix B, finding exact expressions for gauge field correlators, as well as dualization with non-zero Josephson terms which is reported in Appendix E. I was highly involved in writing the paper, especially Sections I–VI and Appendix A–E.
- Paper VII:** *Vortex Sublattice Melting in a Two-Component Superconductor.* I was highly involved in writing the paper. I contributed to the structure factor plots.
- Paper VIII:** *Observation of a metallic superfluid in a numerical experiment.* I was highly involved in writing the paper. I made the framework and did the programming for the 3D vortex grid visualization involving pictures and movies which have been submitted with the paper.

Contents

1	Introduction	1
2	Phase transitions	3
2.1	Free energy	4
2.2	Symmetry breaking	5
2.3	Continuous phase transitions	6
2.3.1	Critical exponents	7
2.3.2	Third moment of the action and finite size scaling	8
2.3.3	Gauge theories	10
2.4	First order phase transitions	11
3	Models and applications	13
3.1	The compact abelian Higgs model	13
3.1.1	Action	13
3.1.2	Dirac strings and magnetic monopoles	15
3.1.3	Confinement-deconfinement phase transition	16
3.2	N -component Ginzburg–Landau model	17
3.2.1	Liquid metallic hydrogen	17
3.2.2	Action	19
3.2.3	Vortex loops and Abrikosov lattice	20
3.2.4	Neutral and charged modes	23
3.2.5	Dual formulation	23
3.2.6	Critical phenomena and phase diagram	25
4	The Monte Carlo scheme	33
4.1	Monte Carlo integration	33
4.2	Importance sampling	34
4.3	The Markov process	35
4.4	The Metropolis algorithm	36
4.5	Measurements	37
4.5.1	Error estimates	38
4.6	Reweighting methods	39
4.6.1	Single histogram reweighting	39

4.6.2	Ferrenberg-Swendsen reweighting	40
4.7	Finite size scaling	43
4.8	First order phase transitions	44

1 Introduction

In 1911 the fascinating phenomenon of *superconductivity* was discovered in mercury by H. K. Onnes [9]. Materials in such a state exhibit exotic characteristics like zero resistivity and perfect diamagnetism. Moreover, in type II superconductors with an external magnetic field present, one observes a lattice of supercurrent tornadoes or vortices each carrying a magnetic flux quantum [10]. In 1957 the theory of superconductivity in ordinary metals, the BCS theory, was proposed [11]. This theory, which by many is considered the most beautiful theory in solid state physics, explained the mechanism of superconductivity to arise from an attractive interaction between pairs of electrons, known as *Cooper pairs*, caused by interactions with the atomic lattice. In metals a large number of electrons can pair up and form a superconducting wave function which extends over the entire sample. Hence, the superconducting state is essentially a *coherent charged condensate* in which we may observe quantum phenomena on a *macroscopic* scale.

Another great achievement in physics was the discovery of superfluid ^4He in 1938 [12,13]. Equivalent to the vortex lattice in superconductors, superfluids exhibit a lattice of superfluid tornadoes when the sample is rotated. Moreover, superfluids are characterized by a *macroscopic* wave function which, in contrast to superconductors, is a *macroscopically coherent charge neutral condensate*.

Until recently materials have been characterized as either superconductors (with a charged condensate) or superfluids (with a neutral condensate). A study of the phenomenological Ginzburg-Landau theory for liquid metallic hydrogen alters this picture [5–8, 14]. Under extreme pressures hydrogen is predicted to form a liquid metallic state in which the electrons and protons decouple and form a two-component liquid [15–17]. This liquid is predicted to form two superconducting condensates, one consisting of electron Cooper pairs and one consisting of proton Cooper pairs [18, 19]. We have found that such a system, which consists of *charged particles*, will exhibit superconducting *and superfluid* properties. This is a novel phenomenon in nature, and puts hydrogen in a new group of materials, namely superconducting superfluids.

The Ginzburg-Landau theory of a system with multiple superconducting condensates which are individually conserved, where the application to liquid metallic hydrogen is a special two-component case, has been studied through a lattice formulation of the

theory [5–8]. Since charges are present the condensate order parameter fields couple to the electromagnetic vector potential known as a gauge field. Lattice gauge theories are studied in various areas of physics such as superconductivity, particle physics, as well as strongly correlated electron systems [20–23]. Even though these systems exhibit completely different physics, the methods for studying model characteristics such as critical properties and phase diagrams are the same in many cases. One example is the quark confinement-deconfinement phase transition in quantum chromodynamics which has an equivalent in quantum phase transitions in strongly correlated electron systems. A two-dimensional system of strongly correlated electrons at zero temperature can be described by an effective lattice gauge theory in 2+1 dimensions [24–34]. In such systems the phase transition from a normal Fermi liquid metallic state to a spin-charge separated state is proposed to be governed by a confinement-deconfinement phase transition. The gauge field in these systems represents strong constraints on the dynamics of the fermions, and is *not* the electromagnetic vector potential.

Monte Carlo integration is a well-suited tool for studying the critical properties of lattice gauge theories beyond all orders in perturbation theory. In the papers [1–4] we have studied lattice gauge theories in 2+1 dimensions as effective theories for zero-temperature quantum phase transitions in strongly correlated electron systems in two-dimensions. We have studied the compact abelian Higgs model as well as abelian Chern-Simons gauge theories and found profoundly rich phase diagrams for which we have mapped out the critical exponents with corresponding universality classes. In the quest for extracting critical exponents we have found that finite size scaling of the *third moment of the action* provides asymptotically correct scaling for practical system sizes and allows us to calculate the critical exponents α and ν . This method was applied extensively for mapping out the phase diagram of the multi-component Ginzburg-Landau theory as well [5–7].

The outline of this thesis is as follows. In Chapter 2 the theory of phase transitions is discussed with emphasis on continuous phase transitions, critical phenomena and phase transitions in gauge theories. In the next chapter the phases of the abelian Higgs model are presented, and the critical phenomena are discussed. Furthermore, the multi-component Ginzburg-Landau theory and the applications to liquid metallic hydrogen are presented. Chapter 4 contains an overview of the Monte Carlo integration scheme, including the Metropolis algorithm, error estimates, and reweighting techniques. This chapter is followed by the papers I-VIII [1–8].

2 Phase transitions

Phase transitions are found in many systems in nature. Some examples are the gas-liquid and liquid-solid transitions in H_2O , the superconducting to normal conductor transition and the superfluid to normal fluid transition. Perhaps the simplest example of a phase transition is the Ising ferromagnet in two dimensions, in which the local magnetization (classical spins) can point up or down. At high temperatures the total magnetization is zero. When temperature is decreased to the Curie critical temperature a majority of the spins point either up or down, producing a net magnetization (shown qualitatively in Figure 2.1, left panel). This spontaneous magnetization is responsible for breaking the up-down symmetry in the uniaxial ferromagnet, and the critical temperature T_c separates the ordered finite magnetization phase from the disordered phase.

Even though the underlying macroscopic theory of systems which exhibit a phase transition can be fundamentally different, it turns out that the properties of phase transitions may qualitatively be the same. Some characteristics of phase transitions are:

- For a given system one can define an ordered phase and a disordered phase, for which there is a value κ_{PT} of some coupling κ which separates the phases. The coupling κ is a physical parameter, e.g. temperature or external magnetic field strength.
- The ordered phase and the disordered phase both have a group of associated symmetry operations, where the symmetry group of the disordered phase is larger than that of the ordered phase. This implies that a symmetry has been broken in the ordered phase. However, this does not apply to systems with local symmetry, gauge theories, because a gauge symmetry is protected by Elitzur's theorem [35]. In these systems the gauge field becomes *massive* in the ordered phase.
- The phase transition is either *continuous*, meaning that the order parameter vanishes continuously at κ_{PT} , a *first order transition* where the order parameter vanishes discontinuously (see Figure 2.1), or a Kosterlitz-Thouless phase transition. In continuous phase transitions critical phenomena are observed and the behavior at these phase transitions can be set in a classification scheme called universality classes.

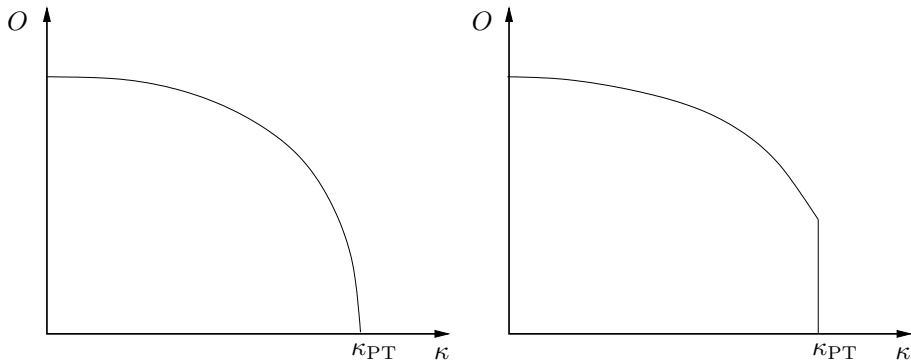


Figure 2.1: The order parameter O as a function of some coupling κ for a continuous phase transition (left panel) and a first order phase transition (right panel). The magnetization order parameter for a two-dimensional lattice of uniaxial (Ising) ferromagnets as a function of temperature is an example of a continuous phase transition.

2.1 Free energy

Phase transitions are observed in statistical mechanical systems, and are a result of collective effects which depend on the elementary interactions in the system. The system Hamiltonian H describes these interactions through potential energy and kinetic energy terms. Temperature is included in the system through the partition function

$$Z = \int \mathcal{D}\Psi \exp(-S), \quad (2.1)$$

which involves the integral over all states Ψ of the system, where the action S is given by $S = \beta H$ and the coupling β is inverse temperature $\beta = 1/T$. The Helmholtz free energy $F(T)$ is defined through $Z = \exp[-\beta F(T)]$, and provides a measure for the energy in the ordered and the disordered state. Moreover, $F(T)$ relates these states to the temperature, and to the elementary interactions through the internal energy $U(T)$,

$$F(T) = U(T) - TS(T) \quad (2.2)$$

where $S(T)$ is the entropy. The internal energy $U(T)$ is the thermal average of the system Hamiltonian. From (2.2) we find that the free energy is minimized by maximizing the entropy of the system and minimizing the internal energy. However, since the internal energy is minimized by ordering the system and the entropy is maximized by disordering the system, there is a order-disorder competition. The outcome of the competition is determined by the temperature. For temperature $T = 0$, $F(T)$ is minimized by minimizing $U(T)$ and hence ordering the system. At high temperatures the

system minimizes the Helmholtz free energy by gaining entropy, and the system is in the disordered state. In many systems, in between these temperature regimes a phase transition temperature T_{PT} exists where the system changes from ordered to disordered. However, phase transitions are collective effects, and for the internal energy $U(T)$ to win the order-disorder competition it is required to have a certain amount of neighbors to interact with. For one-dimensional systems there are only two nearest neighbors to interact with, which is insufficient to produce a globally ordered state. Consequently, one-dimensional systems are always in the disordered state at temperatures $T > 0$.

2.2 Symmetry breaking

In general, the elementary interactions in a physical system can be described fully by the action S . The dynamics are prescribed by a set of evolution equations which follow from varying the action with respect to different degrees of freedom. A symmetry group then corresponds to a set of transformations on the space-time coordinates or the degrees of freedom, which leave the action and thus also the evolution equations invariant.

The two-dimensional Ising model with N spins is given by the action

$$S_{\text{Ising}} = \beta J_0 \sum_{\langle i,j \rangle} \sigma_i \sigma_j \quad (2.3)$$

where $\beta = 1/T$ is the inverse temperature, $J_0 > 0$ is the ferromagnetic coupling, $\langle i, j \rangle$ denotes the sum over nearest neighbors, and the field $\sigma_i \in \pm 1$ represents Ising spins on each lattice site i . Throughout this document we set the Boltzmann constant $k_B = 1$ and $\hbar = 1$. Flipping every spin in the system with the symmetry operation $\sigma_i \rightarrow \tilde{\sigma}_i = -\sigma_i$ leaves the action (2.3) invariant. This global discrete symmetry operation (Z_2) is broken spontaneously at the Curie temperature where the magnetization M defined by the thermal average $M = \frac{1}{N} \langle \sum_i \sigma_i \rangle_\beta$ becomes finite.

An example of a model with a global continuous symmetry ($U(1)$) is the three-dimensional xy model with the action

$$S_{3\text{Dxy}} = -\beta J_1 \sum_{\langle i,j \rangle} \cos(\theta_i - \theta_j) \quad (2.4)$$

with the continuous phase fields θ_i defined on a lattice. The action is invariant under the symmetry operation $\theta_i \rightarrow \tilde{\theta}_i = \theta_i + \chi$ performed on all lattice sites. At the critical temperature all the phases align spontaneously in one direction and the symmetry is broken.

In models with local symmetries (gauge symmetries) the connection between phase transitions and symmetries is more subtle. The lattice London superconductor model

$$S_{\text{London}} = \beta J_2 \sum_{i,\mu} [-\cos(\Delta_\mu \theta_i - A_{i,\mu}) + (\Delta \times A_{i,\mu})^2] \quad (2.5)$$

with a local $U(1)$ symmetry is invariant under the (local) gauge transformation $\theta_i \rightarrow \tilde{\theta}_i = \theta_i + \chi_i$ and $A_{i,\mu} \rightarrow \tilde{A}_{i,\mu} = A_{i,\mu} + \Delta_\mu \chi_i$, where Δ_μ is the lattice difference operator. The theory is the charged version of (2.4). According to Elitzur's theorem the expectation value of any quantity which is not invariant under a gauge transformation, such as $\langle \cos(A_{i,\mu}) \rangle_\beta$, is zero for all couplings (unless one explicitly introduces a gauge fixing term in the theory), and hence a local symmetry cannot be spontaneously broken [35]. Therefore, in the lattice London superconductor model the phases θ_i will not align spontaneously at the phase transition. However, at the critical temperature, the phases and the gauge field conspire to produce a gauge field mass, which is exactly the inverse of the magnetic penetration depth of the superconductor. This phenomenon is known from particle physics as the Higgs mechanism.

Continuous symmetries are related directly to conservation laws of the physical system through Noether's theorem. Noether's theorem states that for every continuous symmetry transformation of a system there is a conservation law. Hence, when a continuous symmetry is broken spontaneously by a phase transition, the corresponding conservation law is violated. Moreover, according to the Hohenberg–Mermin–Wagner theorem models in $d \leq 2$ dimensions with continuous symmetry cannot have a broken symmetry at finite temperature [36, 37].

2.3 Continuous phase transitions

Phase transitions where the order parameter goes to zero in a continuous manner are called continuous, or second order phase transitions (see Figure 2.1). In contrast to a first order phase transition, where two distinct ordered and disordered phases coexists at the phase transition, the ordered and disordered phases in continuous phase transitions are not distinguishable at the critical point.

At continuous phase transitions critical phenomena are observed. The hallmark of critical phenomena is that a correlation length in the system goes to infinity at the critical point. A general scaling Ansatz for the decay of a correlation function $\Gamma(\mathbf{r})$ in a d -dimensional critical system is

$$\Gamma(\mathbf{r}) = \frac{1}{r^{d-2+\eta}} \mathcal{G}(r/\xi) \quad (2.6)$$

where $\mathcal{G}(x)$ is typically a rapidly decaying function such as $\mathcal{G}(x) \sim e^{-x}$, ξ is the correlation length, and η is the anomalous scaling dimension. At the critical point $\xi \rightarrow \infty$ and $\Gamma(\mathbf{r})$ exhibits power law decay. The correlation length ξ which essentially distinguishes the size of the regions which are correlated in the system, will then extend to all length scales. The system is thus scale invariant at the critical point.

Table 2.1: Critical exponents for different physical quantities. Here, h is a (magnetic) field which couples linearly to the order parameter.

Quantity	Symbol	Power law	Temperature regime
Specific heat	C_V	$\propto T - T_c ^{-\alpha}$	$T < T_c$ and $T > T_c$
Order parameter	M	$\propto T - T_c ^\beta$	$T < T_c$
	M	$\propto h h ^{(1-\delta)/\delta}$	$T = 0$
Susceptibility	χ	$\propto T - T_c ^{-\gamma}$	$T < T_c$ and $T > T_c$
Correlation length	ξ	$\propto T - T_c ^{-\nu}$	$T < T_c$ and $T > T_c$
Correlation function	$\Gamma(\mathbf{r})$	$\propto 1/r^{d-2+\eta}$	$T = 0$
Third moment of the action	M_3	$\propto T - T_c ^{-(1+\alpha)}$	$T < T_c$ and $T > T_c$

2.3.1 Critical exponents

A characteristic feature of critical phenomena is that a number of quantities diverge with power law behavior close to the critical point. One example is the specific heat $C_V(T)$ which in the vicinity of a critical temperature T_c follows the power law

$$C_V \sim |T - T_c|^{-\alpha} \quad (2.7)$$

where α is the *critical exponent* of the specific heat. A list of physical quantities and the corresponding critical exponents are given in Table 2.1 [38].

In the early 1970's Kenneth Wilson introduced the renormalization group which provided methods for calculating critical exponents [39]. Furthermore, he found that they should depend on the spatial symmetries, the symmetry of the order parameter and the symmetry and range of interactions, but not on the detailed form and magnitude of interactions. This established the concept of *universality classes*. All the transitions in the same universality class have the same critical exponents. The critical exponents α and ν for some models are listed in Table 2.2. Through dimensionality and scaling analysis one finds relations between critical exponents and the dimensionality d of the physical system, known as *hyperscaling relations*. One such relation is

$$2 - \alpha = \nu d. \quad (2.8)$$

Hyperscaling applies quite generally to transitions that are fluctuation dominated [38], and reduces the number of independent critical exponents in a universality class to two, e.g. β and ν .¹ However, hyperscaling is known to be violated above a critical dimension in spin models and systems with long-range interactions due to the presence of dangerous irrelevant variables [40].

¹The critical exponent of the order parameter β (see Table 2.1) should not be confused with the inverse temperature coupling $\beta = 1/T$.

Table 2.2: The Critical exponents of the specific heat α and the correlation length ν for different models.

Model	α	ν
3D Heisenberg [41]	-0.1336(15)	0.7112(5)
3D xy [42]	-0.0146(8)	0.67155(27)
Inverted 3D xy [42]	-0.0146(8)	0.67155(27)
3D Ising [43]	0.1115(37)	0.6308(10)

2.3.2 Third moment of the action and finite size scaling

At the critical point the singular part F_S of the Helmholtz free energy $F = F_A + F_S$, where F_A is analytic at the critical point, was postulated by Widom [44] to scale as

$$F_S = |\tau|^{2-\alpha} \Phi_{\pm}(h/|\tau|^{\Delta}) \quad (2.9)$$

where $\tau = (T - T_c)/T_c$ is the reduced coupling, Φ_+ and Φ_- are analytical scaling functions above (+) and below (-) T_c respectively, Δ is a scaling exponent and h is a scaling field which is zero at the critical point. The non-analytic part of the specific heat C_V is given by

$$C_V \propto \frac{\partial^2 F_S}{\partial T^2} \propto |\tau|^{-\alpha}. \quad (2.10)$$

The hallmark of a critical point is that the correlation length ξ diverges. For a finite system of size $L \times L \times L$ the correlation length is limited by L so that $\xi \rightarrow L$ at the critical point. Through (2.10) and the power law behavior of ξ around the critical point (see Table 2.1), the specific heat can be related directly to the system size, and at the critical point $C_V \propto L^{\alpha/\nu}$. By measuring C_V at the critical point as a function of system size one can calculate the ratio α/ν . This is known as finite size scaling. However, finite size scaling of C_V provides a measure for the ratio α/ν , and not individual values of α and ν . Moreover, from benchmark studies of finite size scaling of C_V for various models we have found that it is difficult to achieve asymptotically correct scaling of this quantity [2].

A problem arises if $\alpha < 0$, as in the 3D xy model (see Table 2.2). With increasing system size L the peak in C_V will increase. However, since $C_V \propto L^{-|\alpha|/\nu}$ at the critical point, this overall increase will eventually not scale with L . Thus, C_V exhibits a finite cusp which does scale, superposed on a large regular background which eventually will not. Quite typically, impractically large system sizes are needed to eventually distinguish corrections to scaling from actual scaling in C_V , particularly so when $\alpha < 0$.

It would be advantageous to bring out the scaling more clearly relative to confluent singularities, or corrections to scaling. In References [1, 2] we suggest a method to

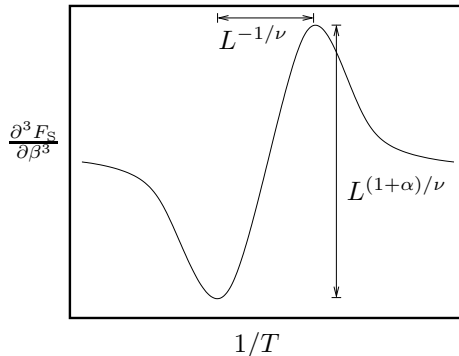


Figure 2.2: The generic shape of the third derivative of the free energy $\frac{\partial^3 F_S}{\partial \beta^3}$ around the critical point. The peak to peak height scales as $L^{(1+\alpha)/\nu}$, and the peak to peak width scales as $L^{-1/\nu}$.

achieve this by taking one further derivative of the free energy with respect to the coupling constant as follows

$$\frac{\partial^3 F_S}{\partial T^3} \propto \frac{\partial^3 F_S}{\partial \beta^3} \propto |\tau|^{-(1+\alpha)}, \quad (2.11)$$

where $\beta = 1/T$. The generic shape of $\frac{\partial^3 F_S}{\partial \beta^3}$ is shown in Figure 2.2. For finite size scaling we relate the third derivative of the free energy (2.11) to the system size through the power law behavior of ξ (see Table 2.1). At the critical point the peak to peak height scales as $L^{(1+\alpha)/\nu}$, whereas the peak to peak width scales as $L^{-1/\nu}$. Consequently, by measuring one quantity, namely $\frac{\partial^3 F_S}{\partial \beta^3}$, as a function of system size we may extract *two* critical exponents. Moreover, this method provides as a test for the hyperscaling relation (2.8).

The third derivative of the free energy (2.11) is related to the action $S = \beta H$ through the partition function Z given in (2.1) such that $F = -\beta^{-1} \ln Z$. Defining the n 'th moment of the action for inverse temperature β as the thermal average $M_n(\beta) = \langle (S - \langle S \rangle)^n \rangle_\beta / V$ we find that [2]

$$\frac{\partial^3 F_S}{\partial \beta^3} \propto \frac{1}{V} \langle (S - \langle S \rangle)^3 \rangle_\beta = M_3(\beta), \quad (2.12)$$

where V is the volume of the system. In Reference [2] we perform benchmark tests of this method for extracting critical exponents α and ν through finite size scaling analysis with Monte Carlo simulations of several models. The simulations of the 2D eight-vertex, the 3D xy, the Ising, and the Ising (Z_2) gauge models give values for α and ν which are in good agreement with the established values for the critical exponents of these

models. The method provides asymptotically correct values for α and ν for practical system sizes.

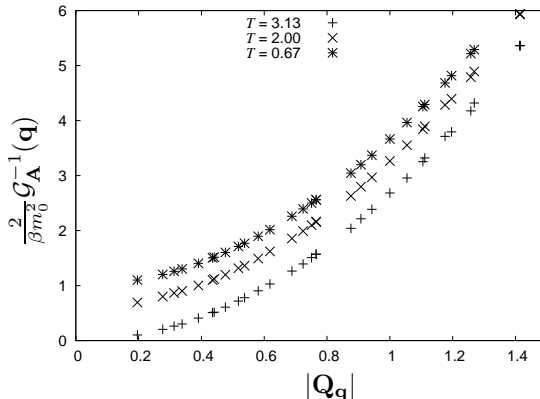


Figure 2.3: Monte Carlo simulation measurements of $\mathcal{G}_A^{-1}(\mathbf{q})$ (defined in (2.13)) as a function of the discrete wave vector \mathbf{Q}_q for the 2-component London superconductor studied in References [5, 6] with $U(1)$ gauge symmetry. For each temperature $T = 1/\beta$ we have plotted $\frac{2}{\beta m_0^2} \mathcal{G}_A^{-1}(\mathbf{q})$ measured from systems of size $L = 8, 12, 20, 32$. The data collapses to a smooth curve. Here, the bare mass m_0 is the low temperature limit of the gauge mass. Following the scaling Ansatz in (2.14), for temperature $T = 3.13$, which is above the critical point $T_c = 2.7(8)$, the values clearly goes to zero as $\mathbf{Q}_q \rightarrow 0$, yielding $m_A = 0$. For temperatures lower than T_c the data points go to a finite value as $\mathbf{Q}_q \rightarrow 0$, and the gauge field is massive. For the lowest temperature $T = 0.67$ the gauge mass is close to the asymptotic value m_0 .

2.3.3 Gauge theories

As was mentioned in Section 2.2 a gauge symmetry is protected by Elitzur's theorem. In theories where the gauge fields are coupled to massive scalar (Higgs) fields, the gauge field can develop a (Higgs) mass (which is a global quantity) at the critical point. The gauge field mass is defined through the Fourier transform of the gauge field correlation function $\mathcal{G}_A(\mathbf{q}) = \frac{1}{V} \langle \mathbf{A}(\mathbf{q}) \cdot \mathbf{A}(-\mathbf{q}) \rangle$ such that [45]

$$\mathcal{G}_A(\mathbf{q}) = \frac{2/\beta}{\mathbf{q}^2 + \Sigma(\mathbf{q})}. \quad (2.13)$$

Close to the critical point we use the following Ansatz for $\Sigma(\mathbf{q})$ proposed by Kajantie *et*

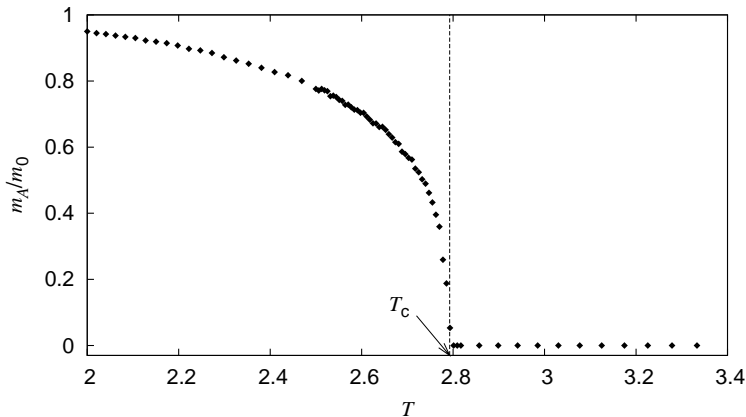


Figure 2.4: The Higgs mechanism in the 2-component London superconductor from Reference [6] with equal bare phase stiffnesses. For each temperature the gauge mass is found by a fit of the function $\mathcal{G}_{\mathbf{A}}^{-1}(\mathbf{q})$ shown in Figure 2.3 to the Ansatz (2.14).

al. [45]

$$\Sigma(\mathbf{q}) = m_{\mathbf{A}}^2 + C|\mathbf{q}|^{2-\eta} + \mathcal{O}(|\mathbf{q}|^{\delta}), \quad (2.14)$$

where $m_{\mathbf{A}}$ is the gauge mass, C is a constant, η is the anomalous scaling dimension defined in (2.6) and $\delta > 2 - \eta$. From the definition $\mathbf{B} \equiv \Delta \times \mathbf{A}$ the gauge mass is identified as the inverse magnetic penetration depth λ . Renormalization group arguments yield $\eta = 4 - d$ at a charged fixed point [46]. Thus, in the limit $q \rightarrow 0$ in $d = 3$ dimensions the equations (2.13) and (2.14) define the gauge mass such that

$$m_{\mathbf{A}}^2 = \lim_{\mathbf{q} \rightarrow 0} \frac{2}{\beta} \mathcal{G}_{\mathbf{A}}^{-1}(\mathbf{q}). \quad (2.15)$$

Taking this limit requires samples of the gauge field propagator for large system sizes for a given coupling β . Such measurements are shown in Figure 2.3. The gauge field mass can then be extracted by a fit to the Ansatz (2.14). Figure 2.4 shows the gauge mass found from such fits which are performed for 76 temperatures across a charged phase transition. This is a clear evidence of the Higgs mechanism.

2.4 First order phase transitions

The liquid-solid phase transition is an example of a first order phase transition. First order phase transitions are characterized by a jump in the order parameter at the temperature $T = T_{\text{PT}}$, as sketched in the right panel of Figure 2.1. Like continuous phase

transitions, the phase transition separates a symmetric high-temperature phase (disordered) and a low-temperature phase where a symmetry is broken (ordered) [47]. However, at a first order phase transition the ordered and disordered phases coexist and unlike continuous phase transitions there is no diverging length scale which leads to scale invariance and critical phenomena. The Helmholtz free energy is given by

$$F(T) = U(T) - T\mathcal{S}(T), \quad (2.16)$$

where the value of the internal energy $U(T)$ can be that of the ordered phase $U_{\mathcal{O}}(T)$ (with $T \leq T_{\text{PT}}$) or that of the disordered phase $U_{\mathcal{D}}(T)$ (with $T \geq T_{\text{PT}}$). Decreasing the temperature from the disordered phase, the internal energy will jump from $U_{\mathcal{D}}(T_{\text{PT}})$ to $U_{\mathcal{O}}(T_{\text{PT}}) \neq U_{\mathcal{D}}(T_{\text{PT}})$ at the phase transition. Over the phase transition the entropy of the system $\mathcal{S}(T)$ has a discontinuity (a jump $\Delta\mathcal{S}$) such that the Helmholtz free energy is continuous at the phase transition. The change in internal energy, which equals $Q = T_{\text{PT}}\Delta\mathcal{S}$, is the latent heat which is transferred out of the system. However, exactly at the phase transition $F(T_{\text{PT}})$ remains unchanged if the system, or parts of it, changes between the two phases. This phenomena of coexisting phases is a hallmark of a first order phase transition.

3 Models and applications

3.1 The compact abelian Higgs model

Lattice gauge theories in 2+1 dimensions serve as effective theories for strongly correlated fermion systems in two spatial dimensions at zero temperature. Phase transitions in such three-dimensional models then correspond to quantum phase transitions in a system at zero temperature in two spatial dimensions. A central issue is whether such systems of strongly correlated fermions can suffer quantum phase transitions from Fermi-liquid metallic states to states where the quasi-particle concept has broken down and given way to singular Fermi liquids [48] or electron-splintered states [49, 50]. Such quantum phase transitions may be related to confinement-deconfinement transitions in 2 + 1 dimensional compact gauge theories. This fact has resulted in focused attention on effective gauge theories of matter fields representing charge doped into Mott-Hubbard insulators, coupled to fluctuating gauge fields representing strong constraints on the dynamics of the fermions on the underlying lattice on which the models are defined [24–34]. Moreover, such models in 2+1 dimensions have been studied as toy models in particle physics [51].

The gauge fields in these models represent strong correlations of the lattice fermions, and the gauge fields are therefore compact. This implies that the gauge fields are 2π periodic, thus each gauge field component is defined in the domain $[-\pi, \pi)$. Compact $U(1)$ gauge theories in 2 + 1 dimensions support stable topological defects in the form of monopole configurations, and it has been suggested that the unbinding of such monopoles, a confinement-deconfinement transition, may be relevant for phenomena such as spin-charge separation in strongly correlated systems [30, 31, 34, 52, 53]. Note that confinement here refers to the confinement of test charges in the problem, not of topological defects of the gauge field (which are space-time instantons, and will hereafter be referred to as "monopole" configurations).

3.1.1 Action

In the papers [1–3] we have studied the abelian $U(1)$ Higgs model with a compact gauge field [54] (Ginzburg–Landau theory with a compact gauge field) coupled minimally to a

$U(1)$ bosonic matter field through the gauge charge q [55–57]. The model is defined by the partition function given by the following functional integral

$$Z = \int_{-\pi}^{\pi} \mathcal{D}\theta \int_{-\pi}^{\pi} \mathcal{D}\mathbf{A} \times \exp \left\{ \beta \sum_{j,\mu} [1 - \cos(\Delta_{\mu}\theta(j) - qA_{\mu}(j))] + \kappa \sum_{P,\mu} [1 - \cos(\varepsilon_{\mu\nu\lambda}\Delta_{\nu}A_{\lambda}(j))] \right\} \quad (3.1)$$

where $\varepsilon_{\mu\nu\lambda}$ is the completely antisymmetric tensor. Moreover, $\sum_{j,\mu}$ denotes a sum over the sites of the lattice, while $\sum_{P,\mu}$ denotes a sum over the plaquettes of the lattice. In (3.1), $\theta(j)$ is the phase of a scalar matter field with unit norm representing holons, Δ_{μ} is the forward lattice difference operator in direction μ , while $A_{\mu}(j)$ is the compact fluctuating gauge field enforcing the on-site constraints reflecting the strong correlations in the problem. In this formulation of the theory we consider the London-limit, where amplitude fluctuations of the matter fields are neglected.

The model (3.1) turns out to have an extremely rich phase diagram in $d = 3$ dimensions. The phase diagram is shown in Figure 3.1. Since the gauge field is compact, the phase diagram is highly dependent on the value of the gauge field charge q . In the case $q = 0$ the matter field decouples completely from the gauge field, and we are left with a 3D xy model and pure Maxwell gauge theory. The former has one critical point of the 3D xy universality class, while the latter is always in the confined state [54]. When $q = 1$, no local order parameter exists for the model, and there is no ordinary continuous phase transition. A confinement-deconfinement transition via Kosterlitz-Thouless monopole unbinding has been discussed [58–60], but conclusive evidence of this has yet to be provided. We have focused on the critical properties of the model with $q \geq 2$, and considered $q = 2$ in detail. In the latter case, the model (3.1) arises as a special limit of a model of two types of bosons living on the sites and the links on a two-dimensional square lattice where the compact gauge field takes care of a local constraint on the number of bosons [61, 62]. For this case we have found that the model clearly exhibits criticality, separating a confined phase from a deconfined phase, with varying critical exponents, indicating a fixed line theory [1–3]. The deconfined Higgs phase corresponds to a fractionalized charge insulator in the original model, whereas the confined phase reflects a conventional Mott insulator [61, 62]. As expected, in the limiting cases $\beta \rightarrow \infty$ and $\kappa \rightarrow \infty$ we find critical exponents α and ν corresponding to the 3D Ising and 3D xy universality classes respectively. In the case $q = 3$ charge is fractionalized in such a way that the excitations carry charge $e/3$, and the situation is reminiscent of the $\nu = 1/3$ fractional quantum Hall effect [63]. This case is particularly interesting because of the existence of a tricritical point where, for values of κ below this point, the transition changes from second order to first order. When $q = 4, 5$ the entire line separating the two phases is critical.

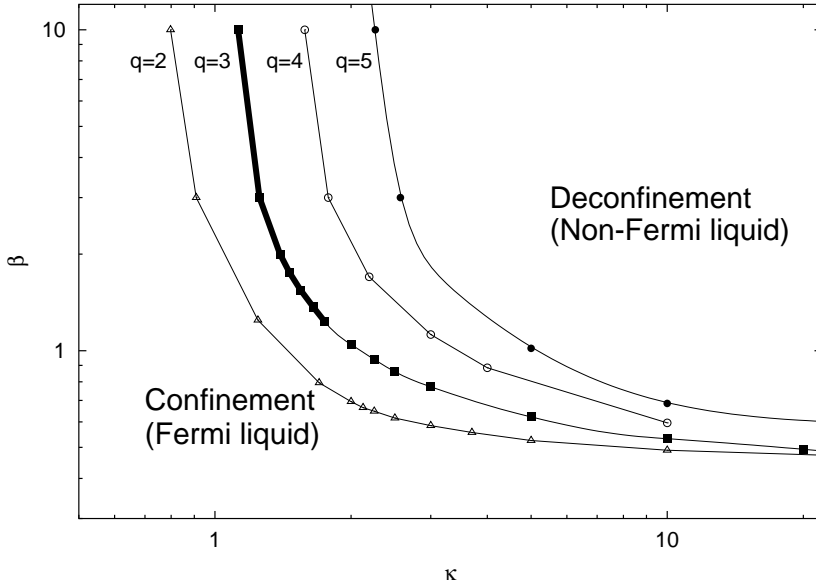


Figure 3.1: The phase diagram of the compact abelian Higgs model in $d = 3$ dimensions for gauge charges $q = 2, 3, 4, 5$, from Reference [2]. For $q = 3$ the phase transition is of first order for $\kappa < \kappa_{\text{tri}}$ (indicated with a thick line). The other lines indicate second order phase transitions. For $q = 2$ the critical exponents vary continuously along the critical line, indicating a fixed line theory.

3.1.2 Dirac strings and magnetic monopoles

The critical properties of the model (3.1) are governed by its elementary excitations which are topological defects in the form of Dirac strings and magnetic monopoles. These objects are stable with respect to a gauge transformation. In the Villain approximation, replacing the cosine terms by periodic quadratic parts, the model may be written in terms of the topological defects as [55]

$$Z = Z_0 \sum_{\{J\}} \sum_{\{Q\}} \delta_{\Delta \cdot \mathbf{J}(j), qQ(j)} \exp \left[-4\pi^2 \beta \sum_{j,k} \left(\mathbf{J}(j) \cdot \mathbf{J}(k) + \frac{q^2}{m^2} Q(j)Q(k) \right) D(j-k; m^2) \right] \quad (3.2)$$

where $m^2 = \beta/\kappa$, and the Green's function $D(j; m^2)$ is given by

$$(-\Delta^2 + m^2)D(j-k; m^2) = \delta_{j,k}. \quad (3.3)$$

Here Z_0 is the partition function for massive spin waves. This is an analytic function, and will not contribute to the critical properties of the theory. The integer Dirac string

field $\mathbf{J}(j)$ represents topological currents as closed loops and open strings. The integer field $Q(j)$, given by the local constraint $\Delta \cdot \mathbf{J}(j) = qQ(j)$ in (3.2), is the monopole charge on the lattice site j . Every open string of the field $\mathbf{J}(j)$ terminates on a magnetic monopole. The constraint implies that the number of Dirac strings entering (exiting) a single positive (negative) magnetic monopole is exactly q .

3.1.3 Confinement-deconfinement phase transition

In the absence of matter fields, compact $U(1)$ gauge theories are known to be permanently confined in $d = 2 + 1$ [54]. This can be measured through the Wilson loop which is a non-local gauge invariant order parameter [56, 64]. In the confinement phase the Wilson loop decays with an area law, implying a linearly confining attraction between test charges, whereas in the deconfinement phase it decays with a perimeter law. The Wilson loop has proven itself to be very useful in the absence of dynamical matter fields to distinguish confined from deconfined phases, but is rendered useless by the presence of them [65]. Hence, the Wilson loop and the related Polyakov loop, are no longer useful order parameters for the model (3.1). Vestergren and Lidmar have suggested a *large Wilson loop* order parameter for the case where the matter field is present [66, 67]. From the dual formulation (3.2) we turn to the continuum formulation for convenience and define the winding number M as

$$M = \int_{\mathcal{S}} \mathbf{J} \cdot d\mathbf{S} \quad (3.4)$$

where \mathbf{J} is the continuum Dirac string field and the surface \mathcal{S} forms a cross section of the system. Let us define the closed path \mathcal{C} on the entire perimeter of \mathcal{S} . Then the order parameter is given by

$$\begin{aligned} \widetilde{W} &= \left\langle \exp \left(i \oint_{\mathcal{C}} \mathbf{A} \cdot d\mathbf{r} \right) \right\rangle = \left\langle \exp \left(i \oint_{\mathcal{S}} \mathbf{B} \cdot d\mathbf{S} \right) \right\rangle \\ &= \left\langle \exp \left(\frac{2\pi i}{q} \oint_{\mathcal{S}} \mathbf{J} \cdot d\mathbf{S} \right) \right\rangle = \left\langle \exp \left(\frac{2\pi i}{q} M \right) \right\rangle \end{aligned} \quad (3.5)$$

since the flux quantum is $\Phi_0 = 2\pi/q$ and hence fractional for $q \geq 2$ [66]. In the deconfinement phase magnetic monopoles are confined in dumb-bell configurations of neutral pairs bound together by q flux lines. In the confinement phase the flux lines condense and percolate through the entire system. This implies that the large Wilson loop decays with an area law in the confinement phase (like the ordinary Wilson loop), but in the deconfinement phase the dumb-bell configurations will cancel out \widetilde{W} on average [66]. This makes the large Wilson loop a suitable confinement-deconfinement order parameter for the model (3.1).

3.2 N -component Ginzburg–Landau model

Under the extreme conditions of pressures around 400 GPa hydrogen H_2 is predicted to dissociate into a metallic fluid of electrons and protons at low temperature [17, 68]. This system is projected to have superconducting phases with one *protonic* and one *electronic* superconducting condensate [15, 18, 19], which can be represented by two complex scalar matter fields minimally coupled to one gauge field in a Ginzburg–Landau theory [5–8, 14, 69, 70]. Since electrons cannot transform into protons and vice versa, the matter field components are individually conserved and there are no Josephson tunneling terms. Moreover, such a model may serve as an effective theory for easy-plane quantum antiferromagnets [71–73]. Furthermore, multicomponent Ginzburg–Landau theories apply to multiband superconductors [74, 75] like MgB_2 where there are two order parameters corresponding to Cooper pairs made up of electrons living on different sheets of Fermi surface. In that case however condensates are not independently conserved and the $U(1) \times U(1)$ symmetry is broken to $U(1)$ (see Appendix E in Reference [6]). We have focused on N -component Ginzburg–Landau theories where Josephson tunneling is forbidden by symmetry [5–8].

3.2.1 Liquid metallic hydrogen

The phase diagram of hydrogen has not yet been explored completely by experiments. For sufficiently high densities it is generally assumed that hydrogen will form a metallic alkali-like crystal [16, 76–78]. A schematic phase diagram is presented in Figure 3.2. For low densities experiments [79, 80] show a H_2 liquid-solid phase transition line with a positive decreasing slope. In Reference [15] this line is predicted to have a negative slope for higher pressures. This prediction is supported in a paper Bonev *et al.* [68] where they also claim to have found evidence of a first order liquid-liquid phase transition from a molecular to a dissociating fluid and predict a triple point at around 300 GPa and 400 K where, above this pressure, the solid is expected to melt into a metallic liquid. A predicted key feature for this metallic liquid at low temperature is the coexistence of superconductivity of proton-proton and electron-electron Cooper pairs [15, 18, 19]. Furthermore, they predict that a metallic quantum fluid will exist at pressures near 400 GPa. High pressure experiments at 320 GPa and 100 K show that hydrogen is then in the insulating solid phase and from these measurements it is predicted that hydrogen will become metallic at around 450 GPa [81]. Hence, there is some consensus about the fact that hydrogen will form a metallic state, but it is still not clear at what pressure it will happen. From high temperature, high pressure shock experiments a conducting fluid state of hydrogen is reported at 140 GPa and 2600 K [82]. Experiments with laser-driven shock waves in a hydrogen sample pre-compressed in a diamond anvil cell produce a conducting fluid state at pressures around 70 GPa with temperatures around 4000 K [83].

To reach the metallic dissociated electron-proton fluid phase at pressures of around 400

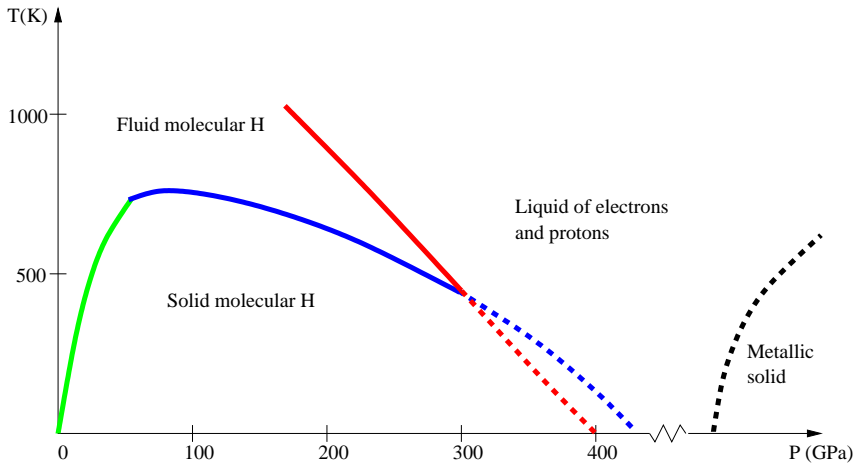


Figure 3.2: A schematic phase diagram of hydrogen. Green line: For pressures up to 44 GPa a molecular hydrogen liquid-solid transition has been proven experimentally [79,80]. Blue line: The predicted continuation of the liquid-solid phase transition line [15,68]. Red line: The insulator to metallic transition line. Black line: A liquid-solid phase transition to a metallic alkali-like crystal state. It is not clear at what pressure this state will form.

GPa for low temperatures is technically extremely demanding. The high pressure physics group at the Lawrence Livermore National Laboratory, USA, led by C. Yoo create a high pressure environment in diamond anvil cells (Figure 3.3). Such experiments are also conducted by a group at the Carnegie Institution of Washington, USA, led by R. Hemley, a group at Harvard University, USA led by I. F. Silvera and a group at Cornell University, USA led by A. L. Ruoff. Being optically transparent, diamond anvil cells are well suited for e.g. optical spectroscopy. Moreover, X-ray measurements, NMR and calorimetry can be performed in these devices. The main limitation in this experimental setup is that the diamonds break at high pressure due to crystal imperfections. However, quite recently great progress has been made at the Carnegie Institution of Washington, USA, in sputtering and microlithography techniques for the production of large single crystal diamonds¹ (Figure 3.4) [86]. This enables the production of large perfect single crystals with good control of the shape of the crystal. High pressure environments for hydrogen at about 450 GPa at low temperatures may therefore be relatively close to experimental realization.

¹The production of large single crystal diamonds at the Carnegie Institution of Washington, D.C., USA was reported in a National Science Foundation (NSF) press release May 16 2005 [84] and in a press release from the Carnegie Institution of Washington the same date [85].

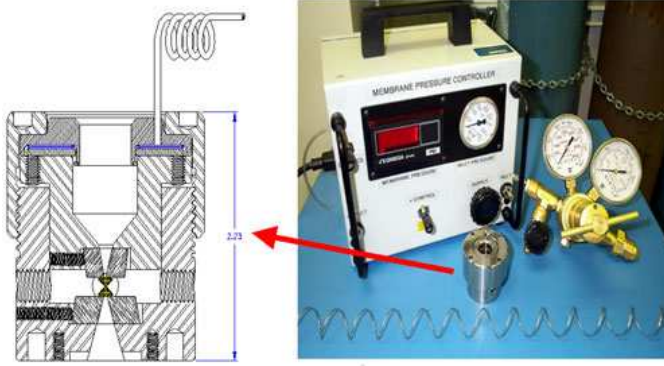


Figure 3.3: The membrane diamond anvil cell (DAC) designed at the Lawrence Livermore Laboratory. Hydrogen is confined between two diamonds. Pressure is applied to the diamonds by injecting inert gas inside a flexible membrane causing it to expand. The membrane expansion applies force to the DAC pistons, and the pressure between the diamonds increases. With this setup the pressure can be controlled very precisely. Credit: Lawrence Livermore National Laboratory, University of California, USA.

3.2.2 Action

We have investigated the phase diagram of a Ginzburg–Landau theory of N individually conserved bosonic matter fields, each coupled to one and the same $U(1)$ non-compact gauge field in 3 dimensions *with no Josephson coupling terms* between order parameter components, with and without an external magnetic field [5–8]. The model is defined by N complex scalar fields $\{\Psi_0^{(\alpha)}(\mathbf{r}) \mid \alpha = 1, \dots, N\}$ each representing superconducting condensates, coupled through the charge e to a fluctuating gauge field $\mathbf{A}(\mathbf{r})$, with the action

$$S = \int d^3\mathbf{r} \left[\sum_{\alpha=1}^N \frac{|(\nabla - ie\mathbf{A}(\mathbf{r}))\Psi_0^{(\alpha)}(\mathbf{r})|^2}{2M^{(\alpha)}} + V(\{\Psi_0^{(\alpha)}(\mathbf{r})\}) + \frac{1}{2}(\nabla \times \mathbf{A}(\mathbf{r}))^2 \right], \quad (3.6)$$

where $M^{(\alpha)}$ is the mass of condensate species α . The potential generally contains terms like

$$\begin{aligned} V(\{\Psi_0^{(\alpha)}(\mathbf{r})\}) = & \sum_{\alpha=1}^N a^{(\alpha)} |\Psi_0^{(\alpha)}|^2 + \sum_{\alpha=1}^N \sum_{\eta=1}^N b^{(\alpha,\eta)} |\Psi_0^{(\alpha)}|^2 |\Psi_0^{(\eta)}|^2 \\ & + \sum_{\alpha \neq \eta} c^{(\alpha,\eta)} (\Psi_0^{(\alpha)})^* \Psi_0^{(\eta)} + \dots \end{aligned} \quad (3.7)$$

where $a^{(\alpha)}$, $b^{(\alpha)}$ and $c^{(\alpha)}$ are real numbers. Assuming that the *individual* condensates are conserved, the potential $V(\{\Psi_0^{(\alpha)}(\mathbf{r})\})$ must be a function of $|\Psi_0^{(\alpha)}(\mathbf{r})|^2$ only, and $c^{(\alpha,\eta)} = 0$ for every α and η .



Figure 3.4: A five carat diamond laser cut from a 10-carat single crystal produced by a high growth rate chemical vapor deposition process produced by researchers at the Carnegie Institution of Washington, D.C., USA. Credit: Carnegie Institution.

3.2.3 Vortex loops and Abrikosov lattice

The critical properties of the model (3.6) are governed completely by the fluctuations of the topological excitations at the critical point. Each condensate is represented by a complex field $\Psi_0^{(\alpha)}(\mathbf{r})$ which can be expressed with an amplitude and a phase, $\Psi_0^{(\alpha)}(\mathbf{r}) = |\Psi_0^{(\alpha)}(\mathbf{r})|e^{i\theta^{(\alpha)}(\mathbf{r})}$. For each condensate $\Psi_0^{(\alpha)}(\mathbf{r})$ the topological defects are vortex loops originating from an integer of 2π windings of the phase $\theta^{(\alpha)}(\mathbf{r})$, defined as

$$\oint_{\mathcal{C}} \nabla\theta^{(\alpha)}(\mathbf{r}) \cdot d\mathbf{l} = 2\pi n^{(\alpha)} \quad (3.8)$$

where \mathcal{C} is a path around the vortex core and $n^{(\alpha)}$ is the winding number. This object is stable with respect to a gauge transformation. For any vortex configuration defined by (3.8), there will be a mathematical singularity in $\nabla\theta^{(\alpha)}(\mathbf{r})$ at the origin. To avoid this singularity the amplitude of the order parameter is defined to go to zero at the origin [38]. For each condensate $\Psi_0^{(\alpha)}$ the Ginzburg–Landau parameter $\xi_{\text{GL}}^{(\alpha)}$ is defined as

$$\xi_{\text{GL}}^{(\alpha)} = \sqrt{\frac{\hbar^2}{2M^{(\alpha)}a_0^{(\alpha)}|\tau|^{-1/2}}} \quad (3.9)$$

where $a^{(\alpha)} = a_0^{(\alpha)}\tau$, $a^{(\alpha)}$ is defined in (3.7), and τ is the reduced mean field temperature. The parameter $\xi_{\text{GL}}^{(\alpha)}$ reflects how the amplitude goes to zero and therefore defines the size of the vortex core for every condensate species α .

If we vary (3.6) with respect to the gauge field \mathbf{A} we obtain the equation for supercurrent

$$\mathbf{J} = \sum_{\alpha=1}^N \left[\frac{ie}{2M^{(\alpha)}} \left\{ \Psi_0^{(\alpha)*} \nabla\Psi_0^{(\alpha)} - \Psi_0^{(\alpha)} \nabla\Psi_0^{(\alpha)*} \right\} + e^2 \left(\frac{|\Psi_0^{(\alpha)}|^2}{M^{(\alpha)}} \right) \mathbf{A} \right]. \quad (3.10)$$

Let us consider a vortex where the phase $\theta^{(\eta)}(\mathbf{r})$ has a 2π winding around the vortex core, while other phase fields do not have nontrivial windings around the core. Expressing \mathbf{A}

from (3.10), and integrating along a path around the vortex core at a distance larger than the magnetic penetration length λ , we obtain an expression for the magnetic flux encompassed by the path given by

$$\Phi^{(\eta)} = \oint \mathbf{A} \cdot d\mathbf{l} = \Phi_0 \frac{|\Psi_0^{(\eta)}|^2}{M^{(\eta)}} \left[\sum_{\alpha=1}^N \frac{|\Psi_0^{(\alpha)}|^2}{M^{(\alpha)}} \right]^{-1}, \quad (3.11)$$

where $\Phi_0 = 2.07 \cdot 10^{-15} \text{Tm}^2$ is the flux quantum. In the case $N > 1$ a single vortex of flavor η will therefore carry fractional flux. Furthermore, such a vortex has a logarithmically divergent energy [5, 6, 70]. Only a *composite* vortex where *all* the phase fields $\theta^{(\alpha)}(\mathbf{r})$ have $2\pi n$ winding around the same vortex core carries integer flux and has finite energy. The composite vortices are responsible for the magnetic properties of the system at low temperatures while thermal excitations in the form of loops of individual fractional-flux vortices are responsible for the critical properties of the system in the absence of an external field. In $N = 1$ -component Ginzburg–Landau theory in finite external magnetic field the ground state is a hexagonal Abrikosov vortex lattice of vortices with unitary flux Φ_0 . Equivalently, in the $N > 1$ -component case with finite external magnetic field the ground state is an Abrikosov vortex lattice of composite vortices with flux Φ_0 [6–8, 14].

We study the model (3.6) on a $d=3$ dimensional cubic lattice with lattice constant $a = 1$. In the lattice formulation the differential operator ∇ becomes a forward difference operator Δ such that

$$\nabla_{\mu} \Psi_0^{(\alpha)} \rightarrow \Delta_{\mu} \Psi_0^{(\alpha)}(\mathbf{r}) = \Psi_0^{(\alpha)}(\mathbf{r} + \mathbf{u}_{\mu}) - \Psi_0^{(\alpha)}(\mathbf{r}) \quad (3.12)$$

where \mathbf{u}_{μ} is the unit vector in direction μ and \mathbf{r} is defined in every lattice point. Furthermore, a lattice equivalent of the definition of the vortex winding number (3.8) must be provided. The vortices are defined on the dual lattice points. A suitable definition of the winding number on the lattice is

$$\sum_{\square} (\Delta_{\mu} \theta^{(\alpha)} - eA_{\mu})_{-\pi, \pi} = 2\pi n^{(\alpha)} \quad (3.13)$$

meaning that the sum around a single plaquette on the lattice must be taken in such a way that on each link in direction μ the quantity $\Delta_{\mu} \theta^{(\alpha)} - eA_{\mu}$ must be forced into the primary interval $[-\pi, \pi)$ by adding integers of $\pm 2\pi$. By this definition gauge invariance of the topological objects is fulfilled. Moreover, since the vortices are defined on the dual lattice points, the problem with a singular vortex origin in the continuum model is avoided by construction. This way the lattice works as a natural ultraviolet cutoff in the system.

To study critical phenomena in the model (3.6) we use the phase-only approximation $\Psi_0^{(\alpha)}(\mathbf{r}) = |\Psi_0^{(\alpha)}| \exp[i\theta^{(\alpha)}(\mathbf{r})]$ where $|\Psi_0^{(\alpha)}|$ is constant for every $\alpha \in [1, \dots, N]$, i.e. we freeze out amplitude fluctuations of *each individual matter field*. The model we

study is therefore the generalization to arbitrary N of the frozen-amplitude one gap lattice superconductor model also known as the London superconductor model [87]. The charged phase transition from a superconductor to a normal conductor is governed by a vortex loop phase transition for which the vortices interact through a screened potential [20, 21]. The phase-only approximation is valid under the assumption that the amplitude of the order parameter fields, whose square gives the density of Cooper pairs, varies insignificantly compared to the fluctuations in the phase at the critical point. For a charged phase transition, which is characterized by short-range vortex interaction, this requirement is met by considering systems where the size of the vortex core is smaller than the lattice spacing whereas the magnetic penetration depth λ is larger than the lattice spacing. Hence, in charged phase transitions the phase-only approximation is only valid for type II superconducting condensates where $\kappa = \lambda/\xi_{GL}$ is large.

The superconducting state emerges when phase coherence of the Cooper pair condensate field sets in. The phase transition from a type II superconductor to the normal state is not driven by the vanishing of the order parameter amplitude. Amplitude fluctuations are a measure of thermal dissociation of Cooper pairs, not of destruction of superconductivity which is defined via long range phase coherence. Moreover, the amplitude of the order parameter is finite across the superconducting phase transition [6, 20, 21]. The phase transition is driven by thermally excited transverse phase fluctuations or vortex loops [21, 88]. Below, we identify one charged mode and $N - 1$ neutral modes in the N -component model (3.6). The critical fluctuations of the charged mode are dominated by the condensate $\Psi_0^{(\eta)}$ with the largest bare phase stiffness $|\Psi_0^{(\eta)}|^2/M^{(\eta)}$. Consequently the *charged* critical sector of the model (3.6) is governed by transverse phase fluctuations in $\Psi_0^{(\eta)}$ alone, and the phase-only approximation for *this* condensate is valid only if $\Psi_0^{(\eta)}$ is a large κ type II superconducting condensate [6]. Moreover, the $N - 1$ neutral vortex modes interact through a long range potential. Generally there are $N - 1$ neutral superfluid phase transitions which are governed by proliferation of long range interacting neutral vortex modes. Therefore, the phase transitions described below, where neutral modes appear, do not significantly depend on whether the corresponding condensates are type I or type II [6]. This can be seen from the following argument. Let us consider the general $N > 1$ case where the bare phase stiffnesses of each condensate are very different. At the lowest critical temperature T_{c1} the critical fluctuations are dominated by the condensate with the lowest bare phase stiffness. Around T_{c1} the gauge field is massive due to the Higgs mechanism which came into play at the highest critical temperature. Hence, the phase transition at T_{c1} is a neutral critical point dominated by fluctuations of the condensate with the lowest bare phase stiffness, the phase only approximation is valid and does not depend on whether this condensate is type I or type II. The behavior of the field with the lowest bare phase stiffness above T_{c1} is not of interest, it is only the remaining fields with higher critical temperatures that matter. We can apply the same argument for all the $N - 1$ neutral critical points, and hence we may use the phase-only approximation with confidence for the corresponding condensate fields.

3.2.4 Neutral and charged modes

In the phase-only approximation the model (3.6) can be rewritten in terms of one charged vortex mode which couples to the gauge field \mathbf{A} and $N - 1$ neutral vortex modes. Before we proceed further, it is useful to give another form of the action² [6]. For brevity let us introduce the bare phase stiffness of the matter field with flavor index α defined as $|\psi^{(\alpha)}|^2 = |\Psi_0^{(\alpha)}|^2/M^{(\alpha)}$, and write the action (3.6) as

$$S = \int d^3\mathbf{r} \left\{ \frac{1}{2\Psi^2} \left(\sum_{\alpha=1}^N |\psi^{(\alpha)}|^2 \nabla \theta^{(\alpha)}(\mathbf{r}) - e\Psi^2 \mathbf{A}(\mathbf{r}) \right)^2 + \frac{1}{2} (\nabla \times \mathbf{A}(\mathbf{r}))^2 \right. \\ \left. + \frac{1}{4\Psi^2} \sum_{\alpha, \beta=1}^N |\psi^{(\alpha)}|^2 |\psi^{(\beta)}|^2 \left(\nabla [\theta^{(\alpha)}(\mathbf{r}) - \theta^{(\beta)}(\mathbf{r})] \right)^2 \right\}, \quad (3.14)$$

where

$$\Psi^2 \equiv \sum_{\alpha=1}^N |\psi^{(\alpha)}|^2. \quad (3.15)$$

The first term in (3.14) represents the charged mode coupling to the gauge field \mathbf{A} , and the remaining terms are the $N - 1$ neutral modes which do not couple to \mathbf{A} . In this formulation it is important to keep in mind that the identification of charged and neutral modes does not imply that the upper terms in (3.14) decouple from the lower terms, they are still coupled through the phase variables $\theta^{(\alpha)}(\mathbf{r})$.

3.2.5 Dual formulation

The identification of charged and neutral modes can be seen very clearly in the dual formulation of the action (3.6), which is explained in detail in Reference [6] (see especially Appendix B). Starting from the lattice formulation of (3.6) with lattice constant $a = 1$ and system size $L \times L \times L$ in the phase-only approximation and introducing inverse temperature $\beta = 1/T$, the action reads

$$S = \sum_{\mathbf{r}} \left\{ -\beta \sum_{\alpha=1}^N |\psi^{(\alpha)}|^2 \sum_{\mu=1}^3 \cos[\Delta_{\mu} \theta^{(\alpha)}(\mathbf{r}) - eA_{\mu}(\mathbf{r})] + \frac{\beta}{2} [\Delta \times \mathbf{A}(\mathbf{r})]^2 \right\}. \quad (3.16)$$

To be able to handle the cosine we use the Villain approximation [89] which essentially approximates the cosine with a harmonic potential which is periodized by the introduction of a new integer valued field. This shifts the critical temperature, but it does not

²See Appendix A in Reference [6] for a detailed description of the identification of charged and neutral vortex modes.

alter the topological excitations of the model or critical properties like critical exponents. In the Villain approximation the partition function reads

$$Z = \int_{-\infty}^{\infty} \mathcal{D}\mathbf{A} \prod_{\gamma=1}^N \int_{-\pi}^{\pi} \mathcal{D}\theta^{(\gamma)} \prod_{\eta=1}^N \sum_{\{\mathbf{n}^{(\eta)}\}} \exp(-S) \quad (3.17)$$

$$S = \sum_{\mathbf{r}} \left[\sum_{\alpha=1}^N \frac{\beta |\psi^{(\alpha)}|^2}{2} (\Delta\theta^{(\alpha)} - e\mathbf{A} + 2\pi\mathbf{n}^{(\alpha)})^2 + \frac{\beta}{2} (\Delta \times \mathbf{A})^2 \right],$$

where $\mathbf{n}^{(\alpha)}(\mathbf{r})$ are integer vector fields ensuring 2π periodicity, and the lattice position index vector \mathbf{r} is suppressed. For $N = 1$ it has been shown that thermal fluctuations in this model excite topological defects in form of closed vortex loops [87]. At the critical temperature the system undergoes a vortex loop proliferation phase transition [21,88,90]. In the vortex representation the partition function is [5, 6]

$$Z = \prod_{\alpha=1}^N \sum_{\{\mathbf{m}^{(\alpha)}\}} \delta_{\Delta \cdot \mathbf{m}^{(\alpha)}, 0} e^{-S_V} \quad (3.18)$$

$$S_V = \pi^2 \sum_{\mathbf{r}, \mathbf{r}'} \sum_{\alpha, \eta} \mathbf{m}^{(\alpha)}(\mathbf{r}) D^{(\alpha, \eta)}(\mathbf{r} - \mathbf{r}') \mathbf{m}^{(\eta)}(\mathbf{r}'),$$

where the integer vector fields $\mathbf{m}^{(\alpha)}(\mathbf{r})$ are defined on the dual lattice and represent vortex segments originating from 2π windings in the corresponding phase fields $\theta^{(\alpha)}(\mathbf{r})$. Here, $\delta_{x,y}$ is the Kronecker-delta, and the discrete Fourier transform [91] of the vortex interaction potential is

$$\tilde{D}^{(\alpha, \eta)}(\mathbf{q}) = 2\beta |\psi^{(\alpha)}|^2 \left[\frac{|\psi^{(\eta)}|^2 / \Psi^2}{|\mathbf{Q}_{\mathbf{q}}|^2 + m_0^2} + \frac{\delta_{\alpha, \eta} - |\psi^{(\eta)}|^2 / \Psi^2}{|\mathbf{Q}_{\mathbf{q}}|^2} \right], \quad (3.19)$$

where Ψ^2 is given by (3.15). Here, the bare mass m_0 is the inverse bare screening length given by $m_0^2 = e^2 \Psi^2$, and $|\mathbf{Q}_{\mathbf{q}}|^2 = \sum_{\mu=1}^3 (2 \sin(q_{\mu}/2))^2$ is the Fourier representation of the lattice Laplace operator, where $q_{\mu} = 2\pi n_{\mu}/L$ with $n_{\mu} \in [1, \dots, L]$. Note that in (3.18) the vortex segments are constrained with $\Delta \cdot \mathbf{m}^{(\alpha)} = 0$ for every flavor $\alpha \in [1, \dots, N]$ on every dual lattice site. This restricts all the integer vortex fields to form closed loops individually.

In the trivial case $e = 0$ the action (3.6) reduces to pure Maxwell theory which has no phase transition and N decoupled 3D xy models. The vortex representation of the interaction potential reduces to

$$\tilde{D}^{(\alpha, \eta)}(\mathbf{q}) = 2\beta |\psi^{(\alpha)}|^2 \frac{\delta_{\alpha, \eta}}{|\mathbf{Q}_{\mathbf{q}}|^2}, \quad (3.20)$$

which is essentially the discrete Fourier transform of the Coulomb interaction. Moreover, (3.20) is exactly the vortex loop interaction matrix of N decoupled neutral 3D xy theories.

The discrete Fourier transform of the vortex interaction matrix (3.19) clearly reflects the existence of neutral and charged vortex modes in the theory. The first term in (3.19) is a Yukawa screened potential, this identifies the charged vortex mode. The second term mediates *long range Coulomb* interactions between vortex fields and identifies the neutral vortex modes. If $N = 1$ the latter cancels out exactly and we are left with the well studied vortex theory of the Ginzburg–Landau model which has a charged fixed point for $e \neq 0$ [46, 92]. For $N \geq 2$ (3.18) is the theory of vortex loops of N flavors interacting through a long range Coulomb potential with an additive screened part.

The above vortex system may be formulated as a continuum field theory [5, 6], introducing N complex matter fields $\phi^{(\alpha)}(\mathbf{r})$ (one for each vortex species), minimally coupled to dual gauge fields $\mathbf{h}^{(\alpha)}(\mathbf{r})$. This generalizes the dual theory for $N = 1$ in Reference [90]. The dual theory reads

$$S_{\text{dual}} = \int d^3\mathbf{r} \left[\sum_{\alpha=1}^N \left(m_{\alpha}^2 |\phi^{(\alpha)}(\mathbf{r})|^2 + |(\nabla - i\mathbf{h}^{(\alpha)}(\mathbf{r}))\phi^{(\alpha)}(\mathbf{r})|^2 + \frac{(\nabla \times \mathbf{h}^{(\alpha)}(\mathbf{r}))^2}{2\beta|\psi^{(\alpha)}|^2} \right) + \frac{e^2}{2\beta} \left(\sum_{\alpha=1}^N \mathbf{h}^{(\alpha)}(\mathbf{r}) \right)^2 + \sum_{\alpha,\eta} g^{(\alpha,\eta)} |\phi^{(\alpha)}(\mathbf{r})|^2 |\phi^{(\eta)}(\mathbf{r})|^2 \right]. \quad (3.21)$$

Here we have written the model back in the continuum formulation, and we have added chemical potential (core-energy) terms for the vortices, as well as steric short-range repulsion interactions between vortex elements. In the $N = 1$ case, an RG treatment of the term $\frac{e^2}{2\beta}\mathbf{h}^2$ yields

$$\frac{\partial e^2}{\partial \ln l} = e^2, \quad (3.22)$$

and hence this term scales up, suppressing the dual vector field \mathbf{h} [5, 6]. The $N = 1$ charged theory in $d = 2 + 1$ therefore dualizes into a $|\phi|^4$ theory and vice versa [92]. Correspondingly, for $N \geq 2$, (3.22) suppresses $\sum_{\alpha=1}^N \mathbf{h}^{(\alpha)}$, but not each individual dual gauge field. For the particular case $N = 2$, assuming the same to hold, the suppression of $\sum_{\alpha=1}^2 \mathbf{h}^{(\alpha)}$ yields that $\mathbf{h}^{(2)} = -\mathbf{h}^{(1)}$ and we end up with a gauge theory of two complex matter fields coupled minimally to one gauge field, which was also precisely the starting point. Thus the theory is self-dual for $N = 2$ [72, 73]. Generally, the dual and the original version of the action describes the same system and the same partition function. This means that they must give the same energy-dependent critical exponents such as α and ν .

3.2.6 Critical phenomena and phase diagram

Elitzur's theorem [35] states that a (local) gauge symmetry cannot be spontaneously broken. This implies that no local order parameter can be defined in a model described

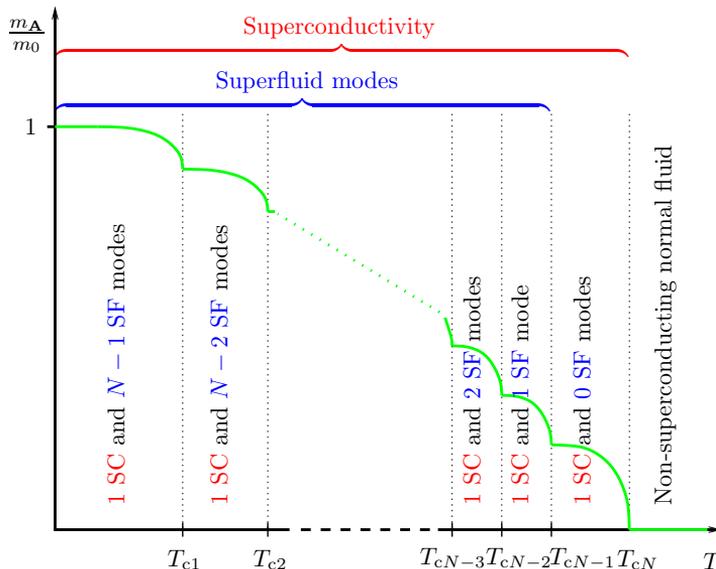


Figure 3.5: Phase transitions in the N -flavor London superconductor with different bare stiffnesses of the N order parameter components in zero magnetic field [6]. There are N critical points. The green line is the gauge field mass $m_{\mathbf{A}}$ in units of m_0 , where m_0 is defined in (3.19). At the highest critical temperature the system becomes superconducting (SC) via a phase transition in the inverted 3D xy universality class. At the lower transitions the system develops neutral superfluid (SF) modes in the superconducting state via a series of $N - 1$ phase transitions, all in the 3D xy universality class.

by a locally gauge invariant action. Hence, probing the phase transition of the charged vortex mode, which is associated with a local gauge symmetry, requires measurements of gauge invariant quantities. To map out the critical properties of the model for $N = 2$ and $N = 3$ we use Monte Carlo simulations to measure the specific heat critical exponent α and the correlation length critical exponent ν through the third moment of the action [2, 5–7] (see Sections 2.3.2 and 4.7). Moreover, we measure the gauge field mass $m_{\mathbf{A}}$ which is the inverse of the London magnetic penetration depth λ and therefore a gauge invariant quantity (see Section 2.3.3) [5, 6]. For finite magnetic field and $N = 2$ we measure the structure factor of the composite Abrikosov lattice as well as the vortex co-centricity. The latter essentially probes the amount of composite vortices in the system. Furthermore, in Reference [8] we sample the superfluid density through the helicity modulus. The critical properties of the action (3.6) are described thoroughly in References [5–8], the main results are presented here.

In zero external magnetic field with $N = 2$ and $N = 3$ complex matter field components with well separated bare phase stiffnesses $|\psi^{(\alpha)}|$ we find one charged critical point and

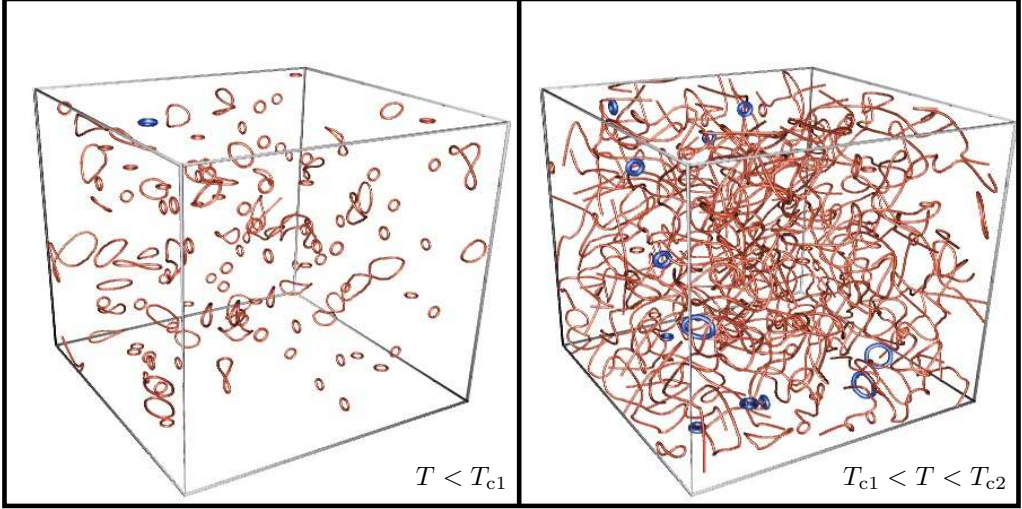


Figure 3.6: Snapshots of the vortex lattice generated from Monte Carlo simulations of the $N = 3$ -component London superconductor model in zero magnetic field with bare phase stiffnesses $|\psi^{(1)}|^2 = 0.33$, $|\psi^{(2)}|^2 = 0.67$, and $|\psi^{(3)}|^2 = 1.33$ [6]. The system experiences three vortex loop proliferation phase transitions at the critical temperatures $T_{c1}, < T_{c2}, < T_{c3}$. **Left panel:** Superconducting state with two superfluid modes. For low temperatures $T < T_{c1}$ there are mostly small vortex loops originating from the condensate $\Psi_0^{(1)}$ (thin red vortices). **Right panel:** Superconducting state with one superfluid mode. At the charged critical point T_{c1} the red vortices proliferate and form loops at all length scales. The vortices which originate from the condensate $\Psi_0^{(2)}$ (thicker blue vortices) appear as small loops.

$N - 1$ neutral critical points. This is partly based on measurements of the critical exponents α and ν which we find to agree with 3D xy values. However, the 3D xy universality class and the *inverted* 3D xy universality class have the same values for α and ν due to duality [92]. To classify the criticalities the gauge field mass $m_{\mathbf{A}} = 1/\lambda$ was measured. A sketch of the results, generalized for arbitrary N and well separated bare phase stiffnesses is shown in Figure 3.5. For high temperatures we find that the gauge mass is zero, corresponding to $\lambda \rightarrow \infty$ and hence a normal state. At the highest critical temperature the gauge mass becomes finite through a second order vortex loop proliferation phase transition. Hence, this is a charged phase transition in the *inverted* 3D xy universality class. In this phase λ is finite, corresponding to a superconducting state. Going further down in temperature we approach $N - 1$ new critical points where the gauge mass has a kink due to a vortex loop proliferation phase transition of neutral modes. These are neutral critical points in the 3D xy universality class. At these

transition points superfluid modes enter the system. *Superfluid states arising in a system of charged particles is a novel property of quantum fluids* [5]. Vortex field snapshots from Monte Carlo simulations of the $N = 3$ model in zero external magnetic field are presented in Figures 3.6 and 3.7.

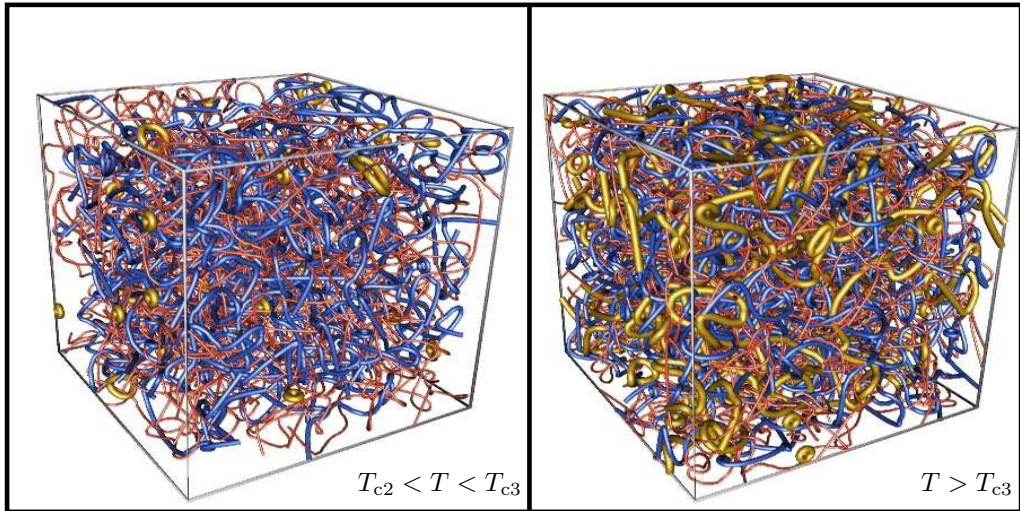


Figure 3.7: Snapshots of the vortex lattice generated from Monte Carlo simulations of the $N = 3$ -component London superconductor model in zero magnetic field with bare phase stiffnesses $|\psi^{(1)}|^2 = 0.33$, $|\psi^{(2)}|^2 = 0.67$, and $|\psi^{(3)}|^2 = 1.33$ [6]. The system experiences three vortex loop proliferation phase transitions at the critical temperatures $T_{c1} < T_{c2} < T_{c3}$. **Left panel:** Superconducting state. The blue vortices proliferate in a plasma of red vortices at the neutral critical point T_{c2} . At the temperature where the snapshot is taken there are small loops of vortices originating from the condensate $\Psi_0^{(1)}$ (thick golden vortices). **Right panel:** Normal state. The golden vortex loops associated with the highest bare phase stiffness proliferate at the neutral critical point T_{c3} , creating a vortex loop plasma of all the vortex components.

In finite magnetic field the $N = 2$ model exhibits phases with no counterpart in the $N = 1$ Ginzburg–Landau model [6]. This is a model for liquid metallic hydrogen where the two condensates represent electron Cooper-pairs and protonic Cooper-pairs where the bare phase stiffnesses are well separated due to the great difference in the mass of the electron and proton. Let us denote the vortices originating from 2π winding in the phase with a large bare phase stiffness $|\psi^{(\alpha)}|$ as *heavy vortices* and the other vortex species as *light vortices*. The phase diagram for a system with $N = 2$ and well separated phase stiffnesses is shown in Figure 3.8. The ground state of the system in external magnetic field is an Abrikosov lattice of composite vortices, as described in Section 3.2.3. This is

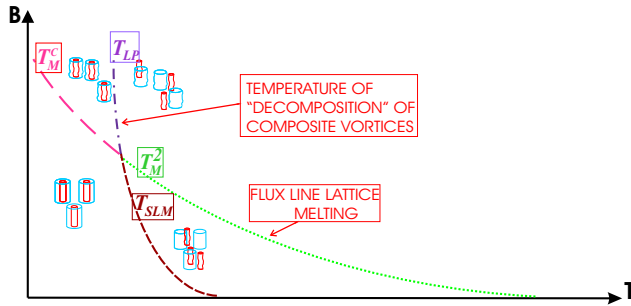


Figure 3.8: A schematic phase diagram of different phases of vortex matter and phase transition lines in the $N = 2$ model in the regime $|\psi^{(1)}| \neq |\psi^{(2)}|$ in finite magnetic field from Reference [6]. At temperatures T_M^c , T_M^2 , and T_{SLM} the melting of the composite vortex lattice, the sublattice of heavy vortices and the sublattice of the light vortices occurs, respectively. At T_{LP} the composite vortices decompose. In the low temperature low magnetic field phase the system is a superconducting superfluid. Superfluidity vanishes upon increasing temperature above T_{SLM} , while the magnetic field is kept low. At T_{SLM} the Abrikosov lattice of the light vortices melts through a vortex loop proliferation phase transition. As temperature is increased further superconductivity is lost as well as at T_M^2 and the Abrikosov lattice of heavy vortices melts [7]. Snapshots of these low field phase transitions are shown in Figure 3.9. Starting from the superconducting superfluid state for higher magnetic field, the system loses superconductivity as temperature is increased beyond T_M^c , and the system is in a superfluid phase. Hence, a purely superfluid phase may arise from two charged condensates. This is a novel phenomenon with no counterpart among known quantum fluids. At the phase transition T_M^c the composite vortex lattice melts, but the composite vortices remain co-centered. As temperature is increased above T_{LP} the system loses superfluidity through a vortex loop proliferation transition of the light vortices [8]. Snapshots of the vortex configurations in these high-field phases are shown in Figure 3.10

a superconducting superfluid state. When the temperature is increased to the critical temperature T_{SLM} the light vortices will tear themselves off the composite vortex lattice in a vortex loop proliferation transition while the heavy vortices remain in a lattice (see Figure 3.9). This is a phase transition in the 3D xy universality class. In this state the system is a superconductor. As temperature is increased further, the heavy vortex lattice will melt in a first order phase transition at T_M^2 . The system is then in the normal state. Upon increasing temperature from the ground state in a high external magnetic field, the composite vortex lattice will melt at T_M^c while the composite vortices still are co-centered (see Figure 3.10). The system then loses superconductivity and is in a superfluid state. The fact that a system of charged condensates can exhibit a superfluid state is a novel phenomenon which has no counterpart among known quantum fluids. As the temperature is increased up to the critical temperature T_{LP} the system undergoes a

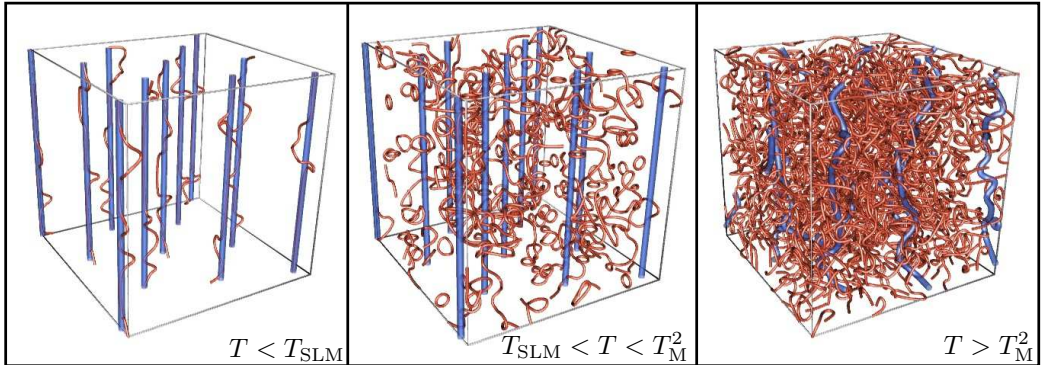


Figure 3.9: Snapshots of the vortex states taken from Monte Carlo simulations of the two-component London superconductor model in a low magnetic field taken at three different temperatures $T = 0.17$ ($T < T_{\text{SLM}}$), $T = 0.37$ ($T_{\text{SLM}} < T < T_{\text{M}}^2$), and $T = 2.38$ ($T > T_{\text{M}}^2$) (see Figure 3.8) [7]. The snapshots are extracted from a small segment ($18 \times 18 \times 18$) of the $L = 96$ vortex system. **Left panel:** Superconducting superfluid phase. For $T < T_{\text{SLM}}$ the vortices are arranged in a co-centered lattice. Protonic (red, thin) and electronic (blue, thick) vortices only perform small excursions from each other. **Middle panel:** Superconducting phase. For $T_{\text{SLM}} < T < T_{\text{M}}^2$ the electronic vortices remain in a lattice. At the critical temperature T_{SLM} the protonic vortex lattice melts through a vortex loop proliferation transition in the 3D xy universality class, and superfluidity is lost. **Right panel:** Normal phase. For $T > T_{\text{M}}^2$ superconductivity is lost due to melting of the electronic vortex lattice at T_{M}^2 .

vortex loop phase transition and becomes a normal fluid.

Experimental realization of liquid metallic hydrogen at low temperatures remains as a great challenge due to the very high pressures which are required. However, the development of techniques for producing very large single diamond crystals for diamond anvil cells will most probably enable sufficiently high pressures [84–86]. Upon realizing low temperature liquid metallic hydrogen the phase diagram Figure 3.8 can be mapped out by measuring superfluidity and superconductivity. The small size of the diamond anvil cells allows rotation of the sample which will produce a vortex lattice similar to what is measured in superfluid helium ^4He . In a finite magnetic field the Abrikosov vortex lattice can be measured by probing magnetic susceptibility with inductive coils [93]. We predict that such measurements on liquid metallic hydrogen in a high magnetic field will reveal a purely superfluid phase where superconductivity is lost. *This is a novel neutral quantum fluid which arises from a charged condensate.* Starting from a superconducting superfluid phase at high fields where the composite vortices form an Abrikosov lattice, the

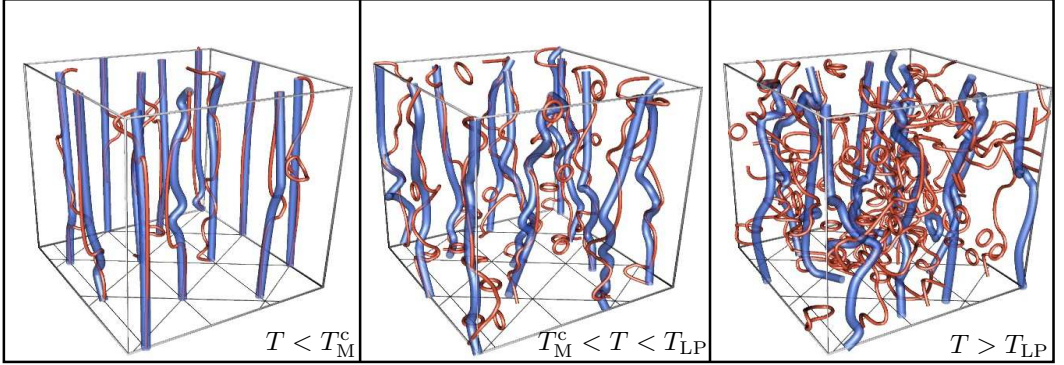


Figure 3.10: Snapshots of vortex states for the two-component London superconductor model in a high magnetic field taken at three different temperatures $T = 0.50$ ($T < T_M^c$), $T = 0.72$ ($T_M^c < T < T_{LP}$), and $T = 0.86$ ($T > T_{LP}$) (see Figure 3.8) [8]. The snapshots are extracted from a small segment ($15 \times 15 \times 15$) of the $L = 120$ vortex system. **Left panel:** Superconducting superfluid phase. For $T < T_M^c$ the vortices are arranged in a co-centered lattice. Protonic (red, thin) and electronic (blue, thick) vortices only perform small excursions from each other. **Middle panel:** Superfluid phase. For $T_M^c < T < T_{LP}$ the composite vortex lattice has melted, and the composite vortices do not stick to the hexagonal lattice which is marked at the bottom of the cube as a guide to the eye. The electronic and protonic vortices perform stronger excursions from each other, but essentially remain co-centered. **Right panel:** Normal phase. For $T > T_{LP}$ the superfluidity is lost in a vortex loop proliferation transition and the electronic and protonic vortices are no longer co-centered.

superfluid phase is found by increasing the temperature such that the composite vortex lattice melts at T_M^c and the composite vortices remain co-centered (see Figure 3.10). This phase transition may be measured from magnetic susceptibility [93]. Upon increasing the temperature, the next phase transition at T_{LP} is more subtle because here the composite vortex lattice is already melted, and the light vortices proliferate. However, this can be measured by flux noise measurements [94]. The phase transition from a superconducting superfluid to a superconductor at T_{SLM} is governed by proliferation of light vortices whereas the heavy vortices remain in an Abrikosov lattice (see Figure 3.9). Since the heavy vortex lattice remains, flux noise measurements should be applied for probing this phase transition as well. Upon increasing temperature the phase transition at T_M^2 where the heavy vortex lattice melts should be detectable from susceptibility measurements [93].

4 The Monte Carlo scheme

The partition function Z introduces the temperature in a statistical mechanical model. Through Z we are able to find expressions for measurable quantities like the specific heat. However, the expressions involve a sum over all states of the system, and it can be a tremendous task to evaluate them, especially in the thermodynamic limit ($V \rightarrow \infty$). A small three-dimensional cubic system of $10 \times 10 \times 10$ Ising spins has $2^{1000} \approx 10^{300}$ states. Today, an ordinary computer can sample about 10^8 such states in 24 hours, which is a very small fraction of the total number of states. To be able to evaluate the partition function within reasonable time the Monte Carlo integration method has been developed.

4.1 Monte Carlo integration

The expectation value $\langle Q \rangle$ of some observable Q for a system at temperature $T = 1/\beta$ with the Hamiltonian H is given by

$$\langle Q \rangle = \frac{\int \mathcal{D}\Psi Q(\Psi) e^{-\beta H(\Psi)}}{\int \mathcal{D}\Psi e^{-\beta H(\Psi)}} \quad (4.1)$$

where the partition function $Z = \int \mathcal{D}\Psi e^{-\beta H(\Psi)}$ is the sum over all states Ψ of the system. Here, $e^{-\beta H(\Psi)}$ are Boltzmann weights, and $e^{-\beta H(\Psi)}/Z$ is the probability that the system is in the state Ψ .

The Monte Carlo method for evaluating integrals such as (4.1) is based on the central limit theorem [95]. Let us consider the following general integral

$$I = \int d^d x f(\mathbf{x}) P(\mathbf{x}) \quad (4.2)$$

where \mathbf{x} is a vector in d -dimensions and $P(\mathbf{x})$ is a probability distribution satisfying the conditions

$$\begin{aligned} P(\mathbf{x}) &\geq 0 \\ \int d^d x P(\mathbf{x}) &= 1. \end{aligned} \quad (4.3)$$

The integral (4.2) can be approximated by evaluating the average of N *independent* samples of the probability distribution $P(\mathbf{x})$

$$X = \frac{1}{N} \sum_{i=1}^N f(\mathbf{x}_i) \Big|_{\mathbf{x}_i \in P(\mathbf{x})} \quad (4.4)$$

where the variable \mathbf{x}_i is sampled according to the function $P(\mathbf{x})$. From the central limit theorem it can be shown that independent of the distribution $P(\mathbf{x})$, $f(\mathbf{x})$ or the dimension d , for large N the average X is normally distributed about I with variance given by the unbiased estimator

$$\text{Var}(X) = \frac{N}{N-1} \left[\frac{1}{N} \sum_i f(\mathbf{x}_i)^2 - \left(\frac{1}{N} \sum_i f(\mathbf{x}_i) \right)^2 \right]. \quad (4.5)$$

This provides as a framework for evaluating integrals such as the expectation value in (4.1). However, the fact that the integral (4.1) can be evaluated through an estimator such as (4.4) does not resolve the problem of an extremely large phase space. The concept of *importance sampling* resolves this.

4.2 Importance sampling

The result above implies that in principle the estimator (4.4) can be evaluated over a set of states Ψ_α which are chosen with equal probability. However, to increase the efficiency of the evaluation we choose to sample the states Ψ_α according to the Boltzmann probability distribution [96]. Then only the states which contribute significantly to the integral (4.1) will be a part of the sum (4.4). Moreover, by choosing the states in this way the variance (4.5) is minimized [95,97]. This is called *importance sampling*. The strategy is to pick N states such that the probability that a particular state Ψ_η is chosen is

$$p(\Psi_\eta) = \frac{e^{-\beta H(\Psi_\eta)}}{Z}. \quad (4.6)$$

Then the estimator for $\langle Q \rangle$ is given by the simple expression

$$\langle Q \rangle = \frac{1}{N} \sum_{\alpha=1}^N Q_\alpha \quad (4.7)$$

where Q_α is the value of Q for a given state Ψ_α . This approach significantly reduces the number of states which are required to evaluate the integral (4.1) with a low signal-to-noise ratio. The next question is how to pick the states according to the Boltzmann probability distribution. The *Markov process* takes care of this.

4.3 The Markov process

The Markov process is the generating engine for the set of states which will be used to evaluate (4.7). Going from a state Ψ_α the Markov process takes the system to a new state Ψ_η in a random fashion. The probability to generate a state Ψ_η given Ψ_α is the transition probability $\mathcal{P}(\Psi_\alpha \rightarrow \Psi_\eta)$. Such probabilities must only depend on the properties of the current states Ψ_α and Ψ_η , and not on any other states the system has passed through. Furthermore, the transition probabilities must satisfy the constraint

$$\sum_{\eta} \mathcal{P}(\Psi_\alpha \rightarrow \Psi_\eta) = 1. \quad (4.8)$$

In a Monte Carlo simulation the Markov process is used repeatedly to generate a *Markov chain* of states. The transition probabilities of the Markov process must be chosen carefully such that when it is run long enough starting from any state it will eventually produce a succession of states which appear with probabilities given by the Boltzmann distribution. When this point is reached we say that the process has come to the equilibrium and the system is warmed up. To be able to reach such states the conditions of *ergodicity* and *detailed balance* must be fulfilled.

In the context of Monte Carlo integration *ergodicity* is the requirement that the Markov process can reach any state of the system from any other state in a finite number of steps in the Markov chain. This enables the Markov chain to reach the true equilibrium and makes it possible to sample the entire phase space.

To ensure that the Boltzmann probability distribution is reached at equilibrium we impose the condition of *detailed balance*. In general, at equilibrium the system must fulfill the following condition

$$\sum_{\eta} p(\Psi_\alpha) \mathcal{P}(\Psi_\alpha \rightarrow \Psi_\eta) = \sum_{\eta} p(\Psi_\eta) \mathcal{P}(\Psi_\eta \rightarrow \Psi_\alpha) \quad (4.9)$$

which means that the rate at which the system makes transitions into and out of any state must be equal. By applying (4.8) to the sum on the left hand side of this expression we find that

$$p(\Psi_\alpha) = \sum_{\eta} p(\Psi_\eta) \mathcal{P}(\Psi_\eta \rightarrow \Psi_\alpha). \quad (4.10)$$

However, this condition is not sufficient to reach the Boltzmann probability distribution. Let us dwell a bit on the reason for this [96]. In Markov process theory, the transition probability $\mathcal{P}(\Psi_\alpha \rightarrow \Psi_\eta)$ is defined as an element of the Markov matrix \mathbf{P} . The probability that the system is in the state Ψ_α at a given step t in the Markov chain is denoted $w_\alpha(t)$. In this notation, the probability that the system is in any state at the step $t + 1$ is given by

$$\mathbf{w}(t + 1) = \mathbf{P}\mathbf{w}(t). \quad (4.11)$$

When the Markov process reaches an equilibrium state at $t \rightarrow \infty$ then

$$\mathbf{w}(\infty) = \mathbf{P}\mathbf{w}(\infty), \quad (4.12)$$

which is just a restatement of (4.10). However, there is nothing prohibiting the system from going to a *dynamic equilibrium* where

$$\mathbf{w}(\infty) = \mathbf{P}^n \mathbf{w}(\infty), \quad (4.13)$$

in which the probability distribution $\mathbf{w}(\infty)$ rotates around a number of different values. Consequently the system is not guaranteed to reach and remain with the desired Boltzmann probability distribution as $t \rightarrow \infty$. To avoid this feature we impose the condition of *detailed balance* on the system

$$p(\Psi_\alpha)\mathcal{P}(\Psi_\alpha \rightarrow \Psi_\eta) = p(\Psi_\eta)\mathcal{P}(\Psi_\eta \rightarrow \Psi_\alpha). \quad (4.14)$$

Clearly, systems which satisfy this condition also satisfy (4.9). The constraint (4.14) means that the rate at which transitions from the state Ψ_α to Ψ_η happen is the same as the reverse. In the case of dynamic equilibrium these rates cannot be the same during the steps t of the Markov chain because the effective transition probability matrix \mathbf{P}^n changes. Hence, through the condition of detailed balance (4.14) the system will come to a stable equilibrium after a sufficient number of Markov steps. Moreover, it can be shown that as $t \rightarrow \infty$, $\mathbf{w}(t)$ will tend exponentially towards the eigenvector corresponding to the largest eigenvalue of \mathbf{P} , and that the largest eigenvalue of \mathbf{P} is one [96]. In matrix form the equilibrium condition (4.10) is

$$\mathbf{p} = \mathbf{P}\mathbf{p} \quad (4.15)$$

which is nothing but the eigenvalue equation for the largest eigenvalue of \mathbf{P} , namely one, with the corresponding eigenvector \mathbf{p} which is the desired Boltzmann probability distribution (4.6). Consequently, as $t \rightarrow \infty$ the probability distribution $w(t)$ will tend to the desired probability distribution \mathbf{p} exponentially in Markov steps.

From the condition of detailed balance (4.14) we find that

$$\frac{\mathcal{P}(\Psi_\alpha \rightarrow \Psi_\eta)}{\mathcal{P}(\Psi_\eta \rightarrow \Psi_\alpha)} = \frac{p(\Psi_\eta)}{p(\Psi_\alpha)} = e^{-\beta[H(\Psi_\eta) - H(\Psi_\alpha)]} \equiv e^{-\Delta S}. \quad (4.16)$$

This leaves us with some freedom in how to choose the transition probabilities. One method of choosing $\mathcal{P}(\Psi_\alpha \rightarrow \Psi_\eta)$ is called the *heat bath* update. We will focus on the traditionally most common method called the *Metropolis algorithm*.

4.4 The Metropolis algorithm

The Metropolis algorithm was constructed to be able to make an ensemble of Boltzmann distributed variables Ψ_α from a set of uniformly distributed numbers [98]. Two very important requirements must be fulfilled namely, ergodicity and detailed balance (4.16).

Within the Metropolis algorithm one starts from an initial state Ψ_0 , and replaces iteratively an old state Ψ_ω by a new one Ψ_ν . Once the equilibrium distribution is reached, repeated applications of the algorithm keeps the states in the same ensemble. The new state should be generated from the old state in such a way that it fulfills the criterion of detailed balance. The Metropolis algorithm has the following set of rules:

1. Generate (randomly) a new candidate state Ψ_ξ .
2. Calculate $\Delta S = -\ln[p(\Psi_\xi)/p(\Psi_\omega)]$.
3. If $\Delta S < 0$ set the new state $\Psi_\nu = \Psi_\xi$.
4. If $\Delta S > 0$ set the new state $\Psi_\nu = \Psi_\xi$ with probability $p(\Psi_\xi)/p(\Psi_\omega)$, otherwise retain the old state $\Psi_\nu = \Psi_\omega$.
5. Do next iteration.

Summarizing the steps 3. and 4. we find that the probability of accepting the candidate Ψ_ξ is given by $\mathcal{P}(\Psi_\omega \rightarrow \Psi_\xi) = \min(1, e^{-\Delta S})$. The reverse transition probability is $\mathcal{P}(\Psi_\xi \rightarrow \Psi_\omega) = \min(1, e^{\Delta S})$. This yields

$$\frac{\mathcal{P}(\Psi_\omega \rightarrow \Psi_\xi)}{\mathcal{P}(\Psi_\xi \rightarrow \Psi_\omega)} = \frac{\min(1, e^{-\Delta S})}{\min(1, e^{\Delta S})} = \begin{cases} \frac{e^{-\Delta S}}{1} = \frac{p(\Psi_\xi)}{p(\Psi_\omega)} & ; \Delta S \leq 0 \\ \frac{1}{e^{\Delta S}} = \frac{p(\Psi_\xi)}{p(\Psi_\omega)} & ; \Delta S \geq 0 \end{cases} \quad (4.17)$$

because $p(\Psi_\alpha)$ is Boltzmann distributed. This shows that the Metropolis algorithm fulfills the detailed balance constraint (4.16).

4.5 Measurements

The Metropolis algorithm implements the concept of importance sampling. Assuming that new states are generated such that ergodicity is fulfilled, the method fulfills the condition of detailed balance and produces an ensemble of Boltzmann distributed states. Measurements of the physical quantity $\langle Q \rangle$ can then be performed using this ensemble, and expectation values are found from the estimator (4.7). From the central limit theorem we know that $\langle Q \rangle$ is normally distributed and we can calculate the variance from (4.5).

However, the Metropolis algorithm usually produces a Markov chain with highly correlated successive states. To get a good estimate of an expectation value we need to sample over many uncorrelated states. To have an idea about over how many uncorrelated states we have sampled, we need to know the correlation time. The correlation time τ is a measure of how many Markov chain steps t it takes the system to evolve between

states that are independent. Mathematically it is defined through the *time-displaced autocorrelation* function

$$\chi(t) = \int dt' [Q(t') - \langle Q \rangle][Q(t' + t) - \langle Q \rangle] \quad (4.18)$$

where $Q(t)$ is the value of the physical quantity Q for the state in step t in the Markov chain. This function will fall off exponentially

$$\chi(t) \sim e^{-t/\tau}, \quad (4.19)$$

which defines the correlation time τ . From Markov matrix theory [96] it can be shown that if the quantity Q is sampled over a number of Markov steps which is much larger than the correlation time, the estimator (4.7) is unbiased with respect to the correlations between states.

4.5.1 Error estimates

An ideal Monte Carlo simulation would produce states where the correlation time is one. In that case the statistical error of a simple quantity like the average is given by the standard variance estimator for normally distributed quantities (4.5). However, often we are interested in the error of much more complicated estimators such as correlation functions. Moreover, in most cases $\tau > 1$ and more sophisticated error estimates are required. The *jackknife* and *bootstrap* methods which include dividing the Monte Carlo data into independent blocks have proven to be excellent for error estimates in such cases [96, 99–101].

Let the quantity Q be measured in a Monte Carlo simulation. Then the jackknife method for finding an error estimate for the expectation value $\langle Q \rangle$ works in the following way:

1. Calculate the $\langle Q \rangle$ from the full data set
2. Divide the data into M blocks (bins) of size much larger than τ .
3. For each block $m \in [1, \dots, M]$ take away the data from block m and calculate $\langle Q \rangle_m$ using all the other blocks.
4. Calculate the error of $\langle Q \rangle$ with the estimator

$$\delta \langle Q \rangle = \sqrt{\frac{M-1}{M} \sum_{m=1}^M (\langle Q \rangle_m - \langle Q \rangle)^2} \quad (4.20)$$

The bootstrap method is closely related to the jackknife method, and is implemented in the following way:

1. Divide the the data into M blocks of size much larger than τ .
2. From the set of M blocks, pick M blocks randomly, not trying to avoid double sampling.
3. Calculate the expectation value of Q using the new data set.
4. Repeat step 2. and 3. a large number of times, each time using an independent set of random numbers to generate the bootstrap sample. The new expectation values are $\langle Q \rangle_1, \langle Q \rangle_2, \dots, \langle Q \rangle_{N_B}$.
5. Find two values a and b such that 68% of $\langle Q \rangle_i$ are within the interval $[a, b]$.
6. The bootstrap error estimate for $\langle Q \rangle$ is then $\delta \langle Q \rangle = (b - a)/2$

4.6 Reweighting methods

The expectation value of quantity Q for a given temperature T can be measured from the estimator (4.7) by implementing the Metropolis algorithm on a computer. However, thorough characterization of the properties of a system around the temperature of a phase transition requires measurements for many temperatures, and hence many Monte Carlo simulations. This can be computationally extremely time consuming. Furthermore, each individual simulation will provide an expectation value for Q with some statistical error, given by (4.5), and to obtain high quality expectation values for quantities which include temperature derivatives, such as the heat capacity (2.10) and the third derivative of the action (2.11), very large Monte Carlo statistics are required. Ferrenberg-Swendsen reweighting was invented to deal with such issues. The technique allows us to perform Monte Carlo simulations for a set of temperatures and estimate values for the observables for temperatures close to the simulated temperatures. Some of the basic ideas were put forward by Valleau and Card [102], but the method in common use today was developed by Ferrenberg and Swendsen [103].

4.6.1 Single histogram reweighting

In order to explain the technique of Ferrenberg-Swendsen reweighting it is instructive to present the single histogram method [104]. Let us say that we have performed a Monte Carlo simulation of a model for the temperature $T_1 = 1/\beta_1$, and for each Markov step t (Monte Carlo sweep) we have saved the energy H_t and the observable Q_t to a file. In general the expectation value of Q for a different coupling β is given by

$$\langle Q \rangle_\beta = \frac{\int \mathcal{D}\Psi Q e^{-\beta H}}{\int \mathcal{D}\Psi e^{-\beta H}} = \frac{\int \mathcal{D}\Psi (Q e^{-(\beta-\beta_1)H}) e^{-\beta_1 H}}{\int \mathcal{D}\Psi (e^{-(\beta-\beta_1)H}) e^{-\beta_1 H}}. \quad (4.21)$$

For the Monte Carlo simulation this is given by the estimator (4.7)

$$\langle Q \rangle_\beta = \frac{\frac{1}{N} \sum_t Q_t e^{-(\beta-\beta_1)H_t}}{\frac{1}{N} \sum_t e^{-(\beta-\beta_1)H_t}} = \frac{\langle Q_t e^{-(\beta-\beta_1)H_t} \rangle_{\beta_1}}{\langle e^{-(\beta-\beta_1)H_t} \rangle_{\beta_1}}, \quad (4.22)$$

where N is the number of Monte Carlo sweeps. By measuring H_t and Q_t at the coupling β_1 for every Monte Carlo sweep, we may in principle find the expectation value of Q at coupling β by applying (4.22). The expression (4.22) can be expressed in terms of energy histograms as well. The Monte Carlo measurements of the energy H_t can be arranged in a histogram $h_{\beta_1}(E)$. Knowing that $h_\beta(E) \propto \rho(E) \exp(-\beta E)$, where $\rho(E)$ is the number of states with energy E (density of states) we can reweight the histogram for another coupling $h_\beta(E) \propto h_{\beta_1}(E) \exp(-(\beta - \beta_1)E)$. If Q is a function of energy $Q(E)$ we may write the histogram reweighted expectation value as

$$\langle Q \rangle_\beta = \frac{\sum_E Q(E) h_\beta(E)}{\sum_E h_\beta(E)} = \frac{\sum_E Q(E) h_{\beta_1}(E) e^{-(\beta-\beta_1)E}}{\sum_E h_{\beta_1}(E) e^{-(\beta-\beta_1)E}}. \quad (4.23)$$

Expressing $\langle Q \rangle_\beta$ like this works when Q is a function of energy. The estimator (4.22) works for any Q .

Note that the method of reweighting the value of Q through (4.22) and (4.23) will eventually break down when β strays too far from β_1 . The Monte Carlo simulation will typically provide an energy histogram which has non-zero values in a relatively small energy range. The tails of the histogram usually contain very few samples. Thus, attempting to calculate a reweighted histogram $h_\beta(E)$ too far from the coupling β_1 will lead to a histogram with either large statistical errors or with many bins without samples. The method of multi histogram reweighting takes care of this and enables us to increase the reweighting coupling range by including Monte Carlo measurements for additional temperatures.

4.6.2 Ferrenberg-Swendsen reweighting

In the Monte Carlo simulation scheme, the probability $p(E)$ of generating a state of total energy E is

$$p(E) = \rho(E) \frac{e^{-\beta E}}{Z_\beta}, \quad (4.24)$$

where $\rho(E)$ is the density of states and Z_β is the partition function for coupling $\beta = 1/T$ sampled over all states of the system. From a Monte Carlo simulation with N measurements of the energy E for coupling β we may estimate $p(E)$ as $p(E) = h_\beta(E)/N$ where $h_\beta(E)$ is the energy histogram for coupling β . By inverting (4.24) this implies that the density of states is $\rho(E) = [h_\beta(E)/N][Z_\beta/\exp(-\beta E)]$. If we perform a number of different simulations with N_i sweeps for different couplings β_i we find correspondingly many estimates of the density of states

$$\rho_i(E) = \frac{h_{\beta_i}(E)}{N_i} \frac{Z_{\beta_i}}{e^{-\beta_i E}}. \quad (4.25)$$

Let us say that we perform a large number of Monte Carlo simulations for the inverse temperature β_i with N_i sweeps and sample $h_{\beta_i}(E)$ for every simulation. Then $\overline{h_{\beta_i}(E)}$ is the energy histogram averaged over all the simulations, and the exact density of states is given by

$$\rho(E) = \frac{\overline{h_{\beta_i}(E)}}{N_i} \frac{Z_{\beta_i}}{e^{-\beta_i E}}. \quad (4.26)$$

To make use of the value of $\rho_i(E)$ for every Monte Carlo simulation we must provide an optimal estimator for the density of states. Each histogram $h_{\beta}(E)$ ranges over a relatively short energy range, but we require an estimate of $\rho(E)$ over the whole energy range covered by the histograms. The estimator should therefore be the weighted average

$$\langle \rho(E) \rangle^w = \frac{\sum_i \rho_i(E) / \sigma_i^2}{\sum_i 1 / \sigma_i^2} \quad (4.27)$$

where σ_i is the standard error of $\rho_i(E)$ and i runs over the number of Monte Carlo simulations. Assuming that the measurements of the energy in the system are independent, the error $\Delta h_{\beta_i}(E)$ should be Poissonian [96, 103]. Hence, $\Delta h_{\beta_i}(E) = (g_i \overline{h_{\beta_i}(E)})^{1/2}$ where $g_i = 1 + 2\tau_i$ where τ_i is the correlation time for Monte Carlo simulation i given by (4.18) and (4.19). The only source of error in (4.25) is the energy histogram $h_{\beta_i}(E)$, and hence the variance σ_i^2 reads

$$\sigma_i^2 = \frac{g_i \overline{h_{\beta_i}(E)}}{N_i^2} \left(\frac{Z_{\beta_i}}{e^{-\beta_i E}} \right)^2 = \frac{g_i \rho(E)^2}{\overline{h_{\beta_i}(E)}}, \quad (4.28)$$

where we have used (4.26) in the last expression. The most optimal estimator for the density of states is thus

$$\langle \rho(E) \rangle^w = \frac{\sum_i \overline{h_{\beta_i}(E)} g_i^{-1} [h_{\beta_i}(E) / N_i] [Z_{\beta_i} / e^{-\beta_i E}]}{\sum_i \overline{h_{\beta_i}(E)} g_i^{-1}} = \frac{\sum_i h_{\beta_i}(E) g_i^{-1}}{\sum_i Z_{\beta_i}^{-1} g_i^{-1} N_i e^{-\beta_i E}} \quad (4.29)$$

where we have used the expression (4.28) in the weighted average (4.27) of $\rho(E)$. In the last expression we have inserted for the average $\overline{h_{\beta_i}(E)}$ from (4.26) which is unknown. The expression (4.29) contains the system partition function for each coupling β_i which we do not know. We get around this by writing up the partition function through (4.29)

$$Z_{\beta_k} = \sum_E \langle \rho(E) \rangle^w e^{-\beta_k E} = \sum_E \frac{\sum_i h_{\beta_i}(E) g_i^{-1}}{\sum_i Z_{\beta_i}^{-1} g_i^{-1} N_i e^{(\beta_k - \beta_i) E}}. \quad (4.30)$$

This equation can be solved by using an iterative method such as the Newton-Raphson method. When the partition function values are found within wanted accuracy the density of states can be calculated through (4.29) and (4.30). Let us say that we have sampled an energy dependent physical quantity $Q(E)$ in the Monte Carlo simulations for every coupling β_i . Then the expectation value of the $Q(E)$ for a coupling β in and around the range of the set of couplings β_i is

$$\langle Q \rangle_\beta = \frac{\sum_E Q(E) \langle \rho(E) \rangle^w e^{-\beta E}}{Z_\beta}. \quad (4.31)$$

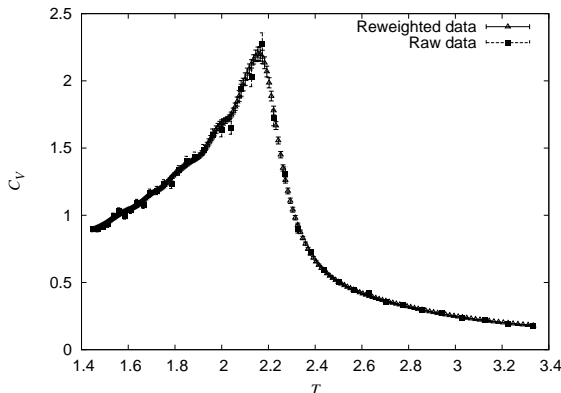


Figure 4.1: Specific heat from Monte Carlo simulations of the 3D xy model for a $12 \times 12 \times 12$ system performed for 40 temperatures with 40000 sweeps for every temperature. The simple average value (4.7) with standard error estimates of the specific heat for each simulation is indicated with squares. Ferrenberg-Swendsen reweighted values for the specific heat for 200 temperatures with jackknife error estimates is indicated by the triangles. Note that the reweighted data is much smoother and has smaller error bars than the raw data.

This reweighting method, called *multi histogram reweighting*, assumes that the measurable quantity Q is a function of the energy E and provides an unbiased expectation value estimator which involves histograms for the energy. The main advantage of this method is that it does not require large computer memory since the Monte Carlo data can be stored in histograms. However, similar expressions have been found for reweighting quantities which do not depend directly on the energy [105]. Let E_i^a be the energy for measurement number a ($a = 1, \dots, N_i$) from Monte Carlo run number i . The expression for the partition function Z_{β_k} becomes

$$Z_{\beta_k} = \sum_i \sum_{a=1}^{N_i} \frac{g_i^{-1} e^{-\beta_k E_i^a}}{\sum_j N_j Z_{\beta_j}^{-1} g_j^{-1} e^{-\beta_j E_i^a}}, \quad (4.32)$$

which should be solved iteratively in a similar fashion as (4.30). The expectation value of Q for coupling β is then

$$\langle Q \rangle_\beta = \sum_i \sum_{a=1}^{N_i} \frac{Q_i^a g_i^{-1} Z_{\beta} e^{-\beta E_i^a}}{\sum_j N_j Z_{\beta_j}^{-1} g_j^{-1} e^{-\beta_j E_i^a}}. \quad (4.33)$$

In the papers [1–8] Ferrenberg-Swendsen reweighting with the expressions (4.32) and (4.33) has been applied to calculate the specific heat and the third moment of the action for a number of models and for different system sizes. The Ferrenberg-Swendsen

reweighting computer program was written by Kari Rummukainen¹. An example of Ferrenberg-Swendsen reweighting of the specific heat for Monte Carlo simulations of the 3D xy model is presented in Figure 4.1. The method provides superior plots for quantities like the specific heat and the third moment of the action, which become much smoother and errors are reduced significantly compared to the expectation value estimator (4.7), simply because Ferrenberg-Swendsen reweighting provides an unbiased expectation value estimator which includes Monte Carlo statistics for several simulations instead of only one and can be calculated for any coupling in the neighborhood of the simulated coupling.

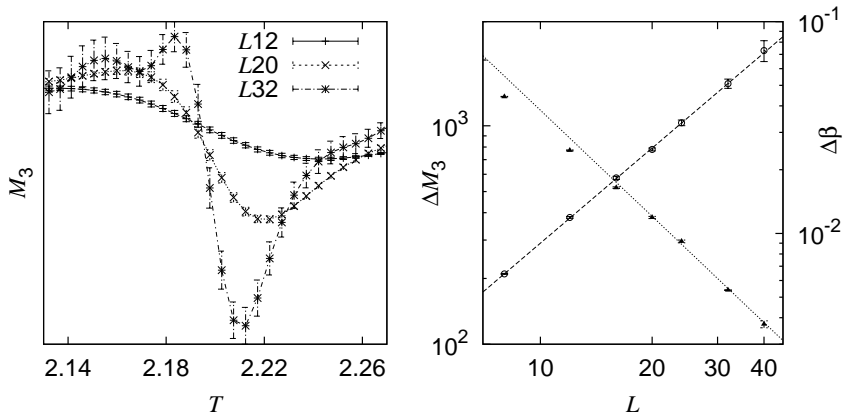


Figure 4.2: **Left panel:** The third moment of the action from Monte Carlo simulations of the 3D xy model for system sizes $L = 12, 20, 32$ published in Reference [2]. Ferrenberg-Swendsen reweighting with jackknife error estimates has been used. **Right panel:** Corresponding third moment of the action finite size scaling plot for the height between the peaks (open circles) and the width between the peaks (filled triangles). From a power law fit using the bootstrap method we find $\alpha = -0.01 \pm 0.01$ and $\nu = 0.67 \pm 0.01$, which confirms that the system is in the 3D xy universality class.

4.7 Finite size scaling

Ferrenberg-Swendsen reweighting is an excellent tool in finite size scaling analysis. The method provides accurate measurements of the third moment of the action (described in Section 2.3.2) accompanied by good error estimates. Finite size scaling of the third moment of the action is shown in Figure 4.2. The reweighted data enables accurate determination of the peak values. From power law fits with bootstrap error estimates we are

¹Reference [106] is the first publication where the program developed by Kari Rummukainen was used, and improvements of the program have been made over a decade.

able to extract the exponents α and ν independently without invoking the hyperscaling relation (2.8).

4.8 First order phase transitions

First order phase transitions are characterized by a jump in the order parameter. However, to distinguish a discontinuity from a continuous drop through Monte Carlo simulations can be quite challenging, especially for weak first order phase transitions which are characterized by very small order parameter jumps [22]. To circumvent these difficulties Lee and Kosterlitz [107] devised a method based on finite size scaling to differentiate between first and second order phase transitions.

A hallmark of first order phase transitions is that the ordered state and the disordered state coexist at the phase transition coupling. As discussed in Section 2.4 these states can coexist because they have the same Helmholtz free energy, and at the phase transition the state of the system will be a mix of ordered and disordered matter. There is a tension associated with the interface between the ordered and disordered parts, and this gives rise to a free energy *barrier* ΔF between the two pure states [47]. By sampling the action of the system one typically finds double peak histograms as in Figure 4.3, which reflects that there are coexisting states.

The probability that an operator X has the particular value x for a system of size L^d is given by

$$P(X = x) = \frac{\sum_{\{\alpha | X_i = x\}} e^{-\beta E_\alpha}}{Z_\beta} = e^{-\beta A(x, L)} \quad (4.34)$$

where $A(x, L)$ is a free energy like quantity which differs from the true free energy by a finite additive quantity. Thus, the difference in $A(x, L)$ between two states is the same as for the free energy

$$A(x, L) - A(x', L) = F(x, L) - F(x', L) = \Delta F(L). \quad (4.35)$$

Here, x and x' are the values of the operator X taken in the two states respectively. The quantity X is usually the energy given by the Hamiltonian of the system. At the phase transition $F(x, L)$ has two pronounced double minima corresponding to two coexisting phases at $X = x_1$ and $X = x_2$ separated by a maximum at $X = x_{\max}$. Therefore, by combining (4.34) and (4.35) we find that the energy gap separating the two pure states is

$$\Delta F(L) = \frac{1}{\beta} \ln \left(\frac{P_{\text{pure state}}}{P_{\text{mixed state}}} \right), \quad (4.36)$$

where $P_{\text{pure state}}$ is the probability to be in one of the minima in $F(x, L)$ and $P_{\text{mixed state}}$ is the probability to be at the maximum of $F(x, L)$, corresponding to one of the two peaks and the minimum between them in the energy histogram respectively (see Figure

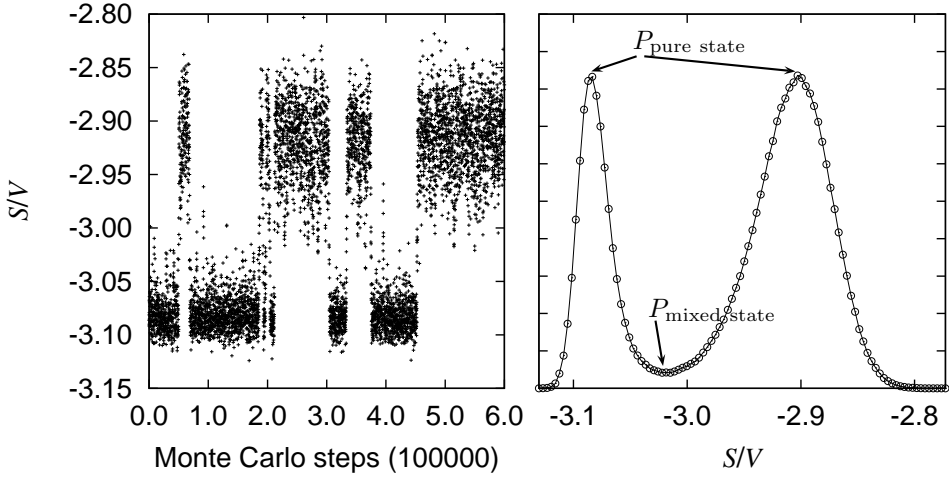


Figure 4.3: Coexisting phases is the hallmark of a first order phase transition. This example is from the Z_3 gauge theory benchmark Monte Carlo simulations for $32 \times 32 \times 32$ system in Reference [2]. **Left panel:** At the phase transition the normalized action S/V as a function of Monte Carlo time jumps between the two energy levels of the ordered and disordered state. **Right panel:** The corresponding S/V histogram clearly shows the coexistence of two phases. The jump in energy between the two peaks is the latent heat of the first order phase transition. The maxima of the histogram reflect the probability to be in either the ordered or the disordered state $P_{\text{pure state}}$, while the minimum inbetween reflects the probability to be in a state with mixed ordered and disordered matter $P_{\text{mixed state}}$.

4.3, right panel). Apart from a normalization factor the energy histogram reflects the probabilities directly. If we consider the scaling of $\Delta F(L)$ it can be shown that $\Delta F(L) \propto L^{d-1}$ corresponds to a first order phase transition, whereas $\Delta F(L) \propto L^0$ corresponds to a second order phase transition [107]. Hence, by measuring energy histogram such as in Figure 4.3 for many system sizes one can determine the order of the phase transition by scaling $\Delta F(L)$ found from (4.36). A scaling with power $d - 1$ corresponds to a flat interface between the two pure states in three dimensions. Hence, proper scaling in three dimensions requires relatively large systems. The method outlined here was applied in Reference [2] to determine the order of the phase transition in the compact abelian Higgs model with gauge charge $q = 3$, which turns out to have a first order transition line which terminates on a tricritical point.

Bibliography

- [1] A. Sudbø, E. Smørgrav, J. Smiseth, F. S. Nogueira, and J. Hove, Phys. Rev. Lett. **89**, 226403 (2002).
- [2] J. Smiseth, E. Smørgrav, F. S. Nogueira, J. Hove, and A. Sudbø, Phys. Rev. B **67**, 205104 (2003).
- [3] F. S. Nogueira, J. Smiseth, E. Smørgrav, and A. Sudbø, Eur. Phys. J. C **33**, 885 (2004).
- [4] E. Smørgrav, J. Smiseth, A. Sudbø, and F. S. Nogueira, Europhys. Lett. **68**, 198 (2004).
- [5] J. Smiseth, E. Smørgrav, and A. Sudbø, Phys. Rev. Lett. **93**, 077002 (2004).
- [6] J. Smiseth, E. Smørgrav, E. Babaev, and A. Sudbø, Phys. Rev. B **71**, 214509 (2005).
- [7] E. Smørgrav, J. Smiseth, E. Babaev, and A. Sudbø, Phys. Rev. Lett. **94**, 096401 (2005).
- [8] E. Smørgrav, E. Babaev, J. Smiseth, and A. Sudbø, submitted to Phys. Rev. Lett. (2005).
- [9] M. Tinkham, *Introduction to Superconductivity* (McGraw-Hill, 1996).
- [10] A. A. Abrikosov, Zh. Eksp. Teor. Fiz. **32**, 1442 (1957).
- [11] J. Bardeen, L. N. Cooper, and J. R. Schrieffer, Phys. Rev. **108**, 1175 (1957).
- [12] P. Kapitza, Nature (London) **141**, 74 (1938).
- [13] J. F. Allen and A. D. Misener, Proc. R. Soc. London, Ser. A **172**, 467 (1939).
- [14] E. Babaev, A. Sudbø, and N. W. Ashcroft, Nature **431**, 666 (2004).
- [15] N. W. Ashcroft, J. Phys.: Condens. Matter **12**, A129 (2000).

-
- [16] N. W. Ashcroft, Condensed matter at higher densities, in *Fenomeni ad alte pressioni, Rendiconti della scuola internazionale di fisica "Enrico Fermi"*, edited by R. J. Hemley and G. L. Chiarotti, Società italiana di fisica, Bologna-Italy, 2002.
- [17] N. W. Ashcroft, *J. Phys. A: Math. Gen.* **36**, 6137 (2003).
- [18] K. Mouloupoulos and N. W. Ashcroft, *Phys. Rev. Lett.* **66**, 2915 (1991).
- [19] K. Mouloupoulos and N. W. Ashcroft, *Phys. Rev. B* **59**, 12309 (1999).
- [20] K. Fosshiem and A. Sudbø, *Superconductivity: Physics and Applications* (John Wiley & Sons, London, 2004).
- [21] A. K. Nguyen and A. Sudbø, *Phys. Rev. B* **60**, 15307 (1999).
- [22] S. Mo, J. Hove, and A. Sudbø, *Phys. Rev. B* **65**, 104501 (2002).
- [23] G. Ripka, hep-ph/0310102 (2003).
- [24] G. Baskaran, Z. Zou, and P. W. Anderson, *Solid State Commun.* **63**, 973 (1987).
- [25] G. Kotliar and J. Liu, *Phys. Rev. B* **38**, 5142 (1988).
- [26] G. Baskaran and P. W. Anderson, *Phys. Rev. B* **37**, 580 (1988).
- [27] L. B. Ioffe and A. I. Larkin, *Phys. Rev. B* **39**, 8988 (1989).
- [28] N. Nagaosa and P. A. Lee, *Phys. Rev. Lett.* **64**, 2450 (1990).
- [29] P. A. Lee and N. Nagaosa, *Phys. Rev. B* **46**, 5621 (1990).
- [30] I. Ichinose and T. Matsui, *Phys. Rev. B* **51**, 11860 (1995).
- [31] I. Ichinose, T. Matsui, and M. Onoda, *Phys. Rev. B* **64**, 104516 (2001).
- [32] R. B. Laughlin, Parallels between quantum antiferromagnetism and the strong interactions, in *Proceedings of the Inauguration Conference of the Asia-Pacific Center for Theoretical Physics*, edited by Y. M. Cho, J. B. Hong, and C. N. Yang, World Scientific, Singapore, 1998.
- [33] D. H. Lee, *Phys. Rev. Lett.* **84**, 2694 (2000).
- [34] N. Nagaosa and P. A. Lee, *Phys. Rev. B* **61**, 9166 (2000).
- [35] S. Elitzur, *Phys. Rev. D* **12**, 3978 (1975).
- [36] P. C. Hohenberg, *Phys. Rev.* **158**, 383 (1967).
- [37] N. D. Mermin and H. Wagner, *Phys. Rev. Lett.* **17**, 1307 (1966).

- [38] P. M. Chaikin and T. C. Lubensky, *Principles of condensed matter physics* (Cambridge University Press, 1995).
- [39] M. E. Fisher, *Rev. Mod. Phys.* **70**, 653 (1998).
- [40] J. Cardy, *Scaling and Renormalization in Statistical Physics* (Cambridge University Press, Cambridge, 1996).
- [41] M. Campostrini, M. Hasenbusch, A. Pelissetto, P. Rossi, and E. Vicari, *Phys. Rev. B* **65**, 144520 (2002).
- [42] M. Campostrini, M. Hasenbusch, A. Pelissetto, P. Rossi, and E. Vicari, *Phys. Rev. B* **63**, 214503 (2001).
- [43] M. Hasenbusch and K. Pinn, *J.Phys. A* **31**, 6157 (1998).
- [44] B. Widom, *J. Chem. Phys.* **43**, 3892 (1965).
- [45] K. Kajantie, M. Laine, T. Neuhaus, A. Rajantie, and K. Rummukainen, *Nucl. Phys. B* **699**, 632 (2004), hep-lat/0402021.
- [46] I. F. Herbut and Z. Tesanovic, *Phys. Rev. Lett.* **76**, 4588 (1996).
- [47] J. Hove, *Critical properties of the Abelian Higgs model*, PhD thesis, NTNU, 2002.
- [48] C. M. Varma, Z. Nussinov, and W. van Saarloos, *Phys. Rep.* **360**, 353 (2002).
- [49] T. Senthil and M. P. A. Fisher, *Phys. Rev. B* **62**, 7850 (2000).
- [50] S. Kivelson, *Synt. Metals* **125**, 99 (2002).
- [51] G. Bhatnot and B. A. Freedman, *Nuclear Physics B* **190**, 357 (1981).
- [52] C. Mudry and E. Fradkin, *Phys. Rev. B* **49**, 5200 (1994).
- [53] C. Mudry and E. Fradkin, *Phys. Rev. B* **50**, 11409 (1994).
- [54] A. M. Polyakov, *Nucl. Phys. B* **120**, 429 (1977).
- [55] M. B. Einhorn and R. Savit, *Phys. Rev. D* **17**, 2583 (1978).
- [56] M. B. Einhorn and R. Savit, *Phys. Rev. D* **19**, 1198 (1979).
- [57] E. Fradkin and S. H. Shenker, *Phys. Rev. D* **19**, 3682 (1979).
- [58] H. Kleinert, F. S. Nogueira, and A. Sudbø, *Phys. Rev. Lett.* **88**, 232001 (2002).
- [59] S. Kragset, A. Sudbø, and F. S. Nogueira, *Phys. Rev. Lett.* **92**, 186403 (2004).
- [60] K. Børkje, S. Kragset, and A. Sudbø, *Phys. Rev. B* **71**, 085112 (2005).
- [61] O. I. Motrunich and T. Senthil, *Phys. Rev. Lett.* **89**, 277004 (2002).

- [62] T. Senthil and O. Motrunich, Phys. Rev. B **66**, 205104 (2002).
- [63] S. D. Sarma, *Perspectives in quantum Hall effects: novel quantum liquids in low-dimensional semiconductor structures* (Wiley, New York, 1997).
- [64] A. M. Polyakov, Phys. Lett. **59B**, 82 (1975).
- [65] Z. Nussinov, J. Zaanen, and A. Sudbø, in preparation .
- [66] A. Vestergren, J. Lidmar, and T. H. Hansson, Europhys. Lett. **69**, 256 (2005).
- [67] A. Vestergren and J. Lidmar, cond-mat/0502533 .
- [68] S. A. Bonev, E. Schwegler, T. Ogitsu, and G. Galli, Nature **431**, 669 (2004).
- [69] E. Babaev, L. D. Faddeev, and A. J. Niemi, Phys. Rev. B **65**, 100512 (2002).
- [70] E. Babaev, Phys. Rev. Lett. **89**, 067001 (2002).
- [71] T. Senthil, L. Balents, S. Sachdev, A. Vishwanath, and M. P. A. Fisher, Phys. Rev. B **70**, 144407 (2004).
- [72] O. I. Motrunich and A. Vishwanath, Phys. Rev. B **70**, 075104 (2004).
- [73] S. Sachdev, Quantum phases and phase transitions of mott insulators, in *Lecture Notes in Physics: Quantum magnetism*, edited by U. Schollwöck, J. Richter, D. J. J. Farnell, and R. A. Bishop, Springer, Berlin, 2004.
- [74] H. Suhl, B. T. Matthias, and L. R. Walker, Phys. Rev. Lett. **3**, 552 (1959).
- [75] A. J. Leggett, Prog. of Theor.Phys. **36**, 901 (1966).
- [76] E. Wigner and H. B. Huntington, J. Chem. Phys. **3**, 764 (1935).
- [77] N. W. Ashcroft, Phys. Rev. Lett. **21**, 1748 (1968).
- [78] H. Mao and R. J. Hemley, Rev. Mod. Phys. **66**, 671 (1994).
- [79] V. Diatschenko *et al.*, Phys. Rev. B **32**, 381 (1985).
- [80] F. Datchi, P. Loubeyre, and R. LeToullec, Phys. Rev. B **61**, 6535 (2000).
- [81] P. Loubeyre, F. Occelli, and R. LeToullec, Nature **416**, 613 (2002).
- [82] W. J. Nellis, S. T. Weir, and A. C. Mitchell, Phys. Rev. B **59**, 3434 (1999).
- [83] P. M. Celliers *et al.*, International Journal of High Pressure Research **24**, 25 (2004).
- [84] National Science Foundation Press Release, May 16, 2005: New technique produces 10-carat diamond, R. Hemley.

-
- [85] Carnegie Institution of Washington, Carnegie Institution News May 16, 2005: Very Large Diamonds Produced Very Fast, R. Hemley.
- [86] R. Hemley, private communication, 2005.
- [87] C. Dasgupta and B. I. Halperin, Phys. Rev. Lett. **47**, 1556 (1981).
- [88] Z. Tesanovic, Phys. Rev. B **59**, 6449 (1999).
- [89] J. Villain, J. Phys. (Paris) **36**, 581 (1977).
- [90] H. Kleinert, *Gauge fields in condensed matter physics, Vol. 1* (World Scientific, Singapore, 1989).
- [91] G. Bachman, L. Narici, and E. Beckenstein, *Fourier and Wavelet Analysis* (Springer, 2000).
- [92] J. Hove and A. Sudbø, Phys. Rev. Lett. **84**, 3426 (2000).
- [93] V. V. Struzhkin, M. I. Erements, W. Gan, H. Mao, and R. J. Hemley, Science **298**, 1213 (2002).
- [94] Ö. Festin *et al.*, Phys. Rev. Lett. **83**, 5567 (1999).
- [95] J. W. Negele and H. Orland, *Frontiers in physics: Quantum Many-Particle Systems* (Addison-Wesley Publishing Company, 1988).
- [96] M. E. J. Newman and G. T. Barkema, *Monte Carlo Methods in Statistical Physics* (Oxford University Press Inc, New York, 1999).
- [97] S. Weinzierl, hep-ph/0006269 (2000).
- [98] N. Metropolis, A. W. Rosenbluth, M. N. Rosenbluth, A. H. Teller, and E. Teller, J. Chem. Phys. **21**, 1087 (1953).
- [99] R. G. Miller, Biometrika **61**, 1 (1974).
- [100] B. Efron, SIAM Review **21**, 460 (1979).
- [101] B. Efron, *The Jackknife, the bootstrap and other resampling plans* (Society for Industrial and Applied Mathematics, 1982).
- [102] J. P. Valleau and D. N. Card, J. Chem. Phys **57**, 5457 (1972).
- [103] A. M. Ferrenberg and R. H. Swendsen, Phys. Rev. Lett. **63**, 1195 (1989).
- [104] A. M. Ferrenberg and R. H. Swendsen, Phys. Rev. Lett. **61**, 2635 (1988).
- [105] E. P. Münger and M. A. Novotny, Phys. Rev. B **43**, 5773 (1991).
- [106] K. Kajantie, L. Kärkkäinen, and K. Rummukainen, Nucl. Phys. B **333**, 100 (1990).
- [107] J. Lee and J. M. Kosterlitz, Phys. Rev. Lett. **65**, 137 (1990).

Paper I

Criticality in the (2+1)-Dimensional Compact Higgs Model and Fractionalized Insulators

Paper II

Phase structure of (2+1)-dimensional compact lattice gauge theories and the transition from Mott insulator to fractionalized insulator

Paper III

Compact $U(1)$ gauge theories in 2+1 dimensions and the physics of low dimensional insulating materials

Paper IV

Phase structure of Abelian Chern-Simons gauge theories

Paper V

Critical Properties of the N-Color London Model

Paper VI

*Field- and temperature induced topological phase transitions in the three-dimensional
N-component London superconductor*

Paper VII

Vortex Sublattice Melting in a Two-Component Superconductor

Paper VIII

Observation of a metallic superfluid in a numerical experiment